

Master Degree course in Physics of Complex Systems

Master Degree Thesis

Water-Induced Stochastic Dynamics of Hydrogen in Soils

Supervisors

Prof. Matteo Bertagni

Prof. Luca Ridolfi

Candidate

Gabriele Nesta

ACADEMIC YEAR 2024-2025

Abstract

Due to the growing interest in hydrogen (H₂) energy for climate change mitigation, hydrogen losses to the atmosphere are expected to increase the H₂ atmospheric concentration over its natural value. The problem is that, for its capacity to interact with atmospheric gases such as methane, ozone and stratospheric water vapor, hydrogen is an indirect greenhouse gas. Hence, a challenging question for the scientific community is: will the use of hydrogen-based energy be a real step toward the solution of climate change or will it effectively add to this already fundamental global issue? To answer this question, a critical piece of the puzzle has to be considered: bacteria in soils. In fact, soil bacteria account for about 80% of the atmospheric hydrogen removal and therefore represent the main global sink of H₂. Many studies on soils and bacterial activity have been performed and multiple factors, both biotic and abiotic, have been found to influence the hydrogen uptake. Above all, soil moisture and, in particular, its temporal fluctuations have been shown to be the dominant control, conditioning both bacterial activity and hydrogen diffusion in the soil.

In this thesis, we try to extend a previous depth-averaged model for moisture and H_2 (Bertagni et al. 2021, Global Biogeochem. Cycles) to the horizontal direction, in order to investigate how spatial heterogeneities and patterns influence hydrogen uptake. A 1D horizontal model is examined, especially to understand the role of horizontal diffusion in this framework and how the various terms governing the hydrogen dynamics in soils are conditioned by it. We show that, while Turing-like instabilities cannot occur in this particular system, spatial heterogeneities and diffusion processes interact to produce complex H_2 uptake patterns. In future works, an extension to 2D models possibly accounting for complex topographies is suggested as a further step, in order to better highlight critical bio-geophysical processes neglected in current formulations. Understanding how hydrogen uptake varies across ecosystems and what types of spatial patterns can arise depending on soil moisture is of crucial importance to comprehend the effects of a possible H_2 energy-based industry in the context of climate change, and this work is a critical step forward in this direction.

Contents

1	Intr	oducti	on	3								
2	0-D	0-Dimensional Dynamics										
	2.1	Couple	ed water and hydrogen dynamics in soils	5								
	2.2		oisture dynamics	6								
		2.2.1	Infiltration	7								
		2.2.2	Losses	9								
	2.3	Soil hy	drogen dynamics	12								
		2.3.1	Atmospheric Flux of Hydrogen	13								
		2.3.2	Biological Decay	14								
	2.4	Simula	ations and results of the model	16								
		2.4.1	Quasi-steady state approximation	16								
		2.4.2	Deposition velocity and limitations	17								
3	Spa	ce-Dep	pendent Dynamics	23								
	3.1	Integra	ating horizontal diffusion processes	23								
	3.2		sis of possible Turing instabilities	24								
		3.2.1	Dimensionless equations	25								
		3.2.2	Conditions for the validity of Turing instabilities	27								
	3.3 1D model											
		3.3.1	Quasi-Steady State Approximation	29 29								
		3.3.2	Cases with a constant D_s	30								
		3.3.3	Cases with a non linear D_s	31								
		3.3.4	α - λ Diagrams	35								
		3.3.5	Check on the validity of the quasi-steady state approximation in 1D	41								
	3.4	2D mo		45								
Δ	of the 1D and 2D Quasi-Steady State Approximation	51										
11	A.1 1D case											
	A.1 A.2		se	51 54								
Bi	bliog	raphy		59								

Chapter 1

Introduction

In the last decades, with the worsening of the climate change problem, an alternative to fossil fuels has been strongly looked for and, among the various solutions, hydrogen-based energy has received growing interest from the scientific community. However, an eventual and massive use of hydrogen-based energy could also be problematic since leakages toward the atmosphere are expected to increase considerably the concentration of H₂ above its actual level of about 530 ppb. For its capacity to easily react with other atmospheric gases such as methane, ozone and water vapor, hydrogen is an indirect greenhouse gas and an increase in its atmospheric concentration could produce undesired effects. Therefore, if, on one hand, hydrogen energy is a clean and easily available type of energy, on the other, its vast employment on a global scale could generate opposite results and further intensify the global warming. It is, thus, of crucial importance to understand in a deeper way the natural cycle of H₂ on our planet. In this context, soil plays a leading role as its layers harbour large communities of bacteria and microorganisms whose metabolism is based on hydrogen, which they acquire through H₂-oxidizing enzymes. Their biological activity is responsible for about 80% of the total hydrogen removal, which makes soil the main global sink of the atmospheric H₂. In light of these facts and that these bacterial communities are found in nearly every ecosystem, the study of the hydrogen dynamics in soils is of clear importance in understanding whether a future use of H₂-based energy could be beneficial or not.

Previous works, recalled in the second chapter of this thesis, have already highlighted the main factors that influence and control the hydrogen dynamics in soils. Above all, soil moisture and its temporal fluctuations are the dominant parameters which could enhance or hinder the hydrogen uptake the most. In fact, soil moisture conditions both the activity of the bacterial communities, which can enter a dormant state if a prolonged lack of water (such as in hyper-arid ecosystems) occurs, and the atmospheric flux of H₂. If the level of water in soil is too high, in fact, hydrogen flows from atmosphere to soil with much more difficulties. Due to its low solubility in water, the H₂ available in soils is mostly in the gas phase and can diffuse in the vertical direction only if the soil pores are free from water.

Soil moisture, in turn, strongly depends on rain events whose unpredictable and stochastic nature adds to the complexity of the models, further complicated by the action

of many other secondary actors: temperature, salinity and pH of the soil impact significantly on the hydrogen uptake, as well as the presence of layers of material, like snow or litter, that could cover the soils and hinder even more the atmospheric flux of H₂.

Until now, these models have just taken the temporal variability into account, neglecting the horizontal spatial variables. Only on a global scale, due to changes in temperature and precipitation rates among the various ecosystems, has spatial variability been investigated.

The aim of this thesis is to extend these previous works by adding the dependencies on the x and y directions, whose effects are examined, especially, on the local scale. As a consequence, another phenomenon has to be added to our discussion: the horizontal diffusion of both moisture and hydrogen. Its impacts on the model are studied in detail, investigating whether heterogeneous spatial patterns in the H_2 uptake can be induced by diffusion processes. After having analysed, for a generic dimensionality, whether Turing-like instabilities can arise in our model, a 1D case is thoroughly treated, whose simulations and results are examined in the third chapter. Furthermore, a discussion about the different behaviors of soil moisture and hydrogen concentration in several hydrologic regimes is carried out to better underline how diffusion and rain events interact with each other to generate peculiar spatial profiles depending on which ecosystem we are in. Finally, we end this work with an introductory extension to a 2D model, where a couple of more and more realistic scenarios are presented.

This study is a further step in the comprehension of how hydrogen uptake changes across ecosystems. Also, from a mathematical point of view, we extend a previous ordinary differential method to a partial one, which could better describe spatial variability on the local scale. The latter scale, neglected in previous models, is of fundamental importance to understand how local heterogeneity and spatial patterns, summed up together, can influence the H₂ uptake on the global scale.

Chapter 2

0-Dimensional Dynamics

2.1 Coupled water and hydrogen dynamics in soils

The starting points are the two coupled equations that describe the dynamics of moisture and hydrogen in the soil, which are the main variables of study in this work. Before going on with their description, we must underline that horizontal homogeneity will be assumed in this first chapter, neglecting, in other words, the dependence on x and y. In the next chapter, instead, we are going to relax this approximation precisely to investigate the role of the horizontal spatial variables on our model.

For the hydrogen dynamics, hence, the balance equation is:

$$\frac{\partial}{\partial t}(\Theta c) = -\frac{\partial}{\partial z}\phi + p - bd \tag{2.1}$$

where t is the time and z is the vertical axis pointing downward; $\Theta(t,z)$ is the soil volumetric air content (measured in cm_{air}^3/cm_{soil}^3) and c(t,z) is the hydrogen concentration in the atmosphere (measured in $moles/cm_{air}^3$) so that the product $\Theta c = c_s$ is the hydrogen concentration in soil (measured in $moles/cm_{soil}^3$); $\phi(c,\theta,\delta)$ gives us the hydrogen flux between the atmosphere and the soil. It mainly depends on c,θ , which is the water volumetric content (and is given by the other equation), and on δ , which is the depth of the possible diffusive barriers, such as snow, litter or other materials which can accumulate on the soil and hinder the hydrogen flux. p is the term that stands for the hydrogen production inside the soil, whereas bd is the consumption term that represents the biological decay of the hydrogen inside the soil (biological since they are some microorganisms that are responsible for the hydrogen depletion).

For the equation that describes the soil-water balance, we have:

$$\frac{\partial}{\partial t}\theta = -\frac{\partial}{\partial z}\psi + \sigma(z) \tag{2.2}$$

where the new terms are ψ that is the vertical flux of water per unit area and $\sigma(z)$ which represents the plant uptake of water.

It is convenient to average these two equations along the vertical direction and this can be done following the procedure explained in "Bertagni et al. (2021)" [1]. Thus, after

integrating over a depth Z, the resulting equations are:

$$nZ\frac{d}{dt}\overline{s} = R + J - I - Q - ET - L \tag{2.3}$$

$$nZ\frac{d}{dt}[(1-\overline{s})\overline{c}] = F + Z \cdot (P - BD)$$
 (2.4)

where \bar{s} and \bar{c} stand for the vertical averages, respectively, of s and c. In the derivation of the above equations, we have used the relations $\theta = n \cdot s$ and $\Theta = n(1-s)$ introducing two new variables: s(z,t), the relative soil moisture, and n, the soil porosity (defined as $n = \theta + \Theta$). s, in particular, will play a crucial role in the subsequent analysis and, together with c, will be the main variable in this discussion.

In the following sections, we are going to describe in detail all the terms involved in the previous equations. Here we only list their names: in the first equation R(t) is the rainfall, J(t) is the irrigation (that we will no longer consider in the following), I(t) is the canopy interception, $Q(\overline{s})$ is the surface runoff, $ET(\overline{s})$ is the evapotranspiration loss, $L(\overline{s})$ is the leakage; in the second equation F is the hydrogen flux, P is the averaged production term and BD is the averaged biological decay term.

2.2 Soil moisture dynamics

The difficulties in solving Eq. (2.3) and (2.4) come from the fact that s depends on stochastic events: rains. So, we have to be quite careful in modeling the various terms of Eq. (2.3). For this reason, we will follow the analysis of "Laio et al. (2001)" [5]. In particular, we divide, as they suggest, the terms into two categories: those that contribute to the rate of infiltration $\varphi[s(t),t]$ and those that determine the losses $\chi[s(t)]$, so that we can rewrite Eq. (2.3) as

$$nZ\frac{d}{dt}s(t) = \varphi[s(t), t] - \chi[s(t)]$$
(2.5)

where, for the sake of simplicity, we denote with s the average along z of the soil moisture, namely \bar{s} .

The rate of infiltration $\varphi[s(t),t]$ is the actual quantity of water, due to rainfall, that reaches the soil and is absorbed. We can, then, write it as

$$\varphi[s(t), t] = R(t) - I(t) - Q[s(t), t] \tag{2.6}$$

where R(t) represents the rainfall rate; I(t) is the quantity of rainfall intercepted by canopy cover and, for this reason, not reaching the soil; Q[s(t),t] stands for the rate of runoff, that is the part of rainfall that can't be absorbed because the soil is already saturated.

The losses $\chi[s(t)]$, instead, tell us how soil moisture decreases over time due to different factors. These are mainly evapotranspiration, that is the sum of evaporation of water from the soil and plants transpiration, and leakage, which is the infiltration due to gravity from the soil layer under consideration to the deeper soil layers. So, we can express $\chi[s(t)]$ as

$$\chi[s(t)] = ET[s(t)] + L[s(t)] \tag{2.7}$$

where, as we said, ET and L are, respectively, the rate of evapotranspiration and leakage.

2.2.1 Infiltration

To model this term, we will assume that the rainfalls are independent from the soil and its moisture, and hence that they are external forces acting on our system. They are also, and more importantly, stochastic events both in the occurrence and in the amount of water fallen. To model the former, we consider the times of rains as a Poisson process, so as a series of temporal events separated by a time quantity τ that we extract from an exponential distribution with mean $1/\lambda$. We also consider that rains are instantaneous events, neglecting their actual duration and concentrating the whole precipitation in a single instant of time during a particular day.

For the amount of rain (represented here with the random variable h), we again extract the values of h from an exponential distribution, but with a different mean, α . Physically, α is the mean depth of rainfall events and is measured in cm.

So we have two exponential distributions one for the time distances between subsequent rainfalls and the other for the quantity of water fallen while it rains. We can write them as

$$f_H(h) = \frac{1}{\alpha} e^{-h/\alpha} \quad \text{for} \quad h \ge 0$$
 (2.8)

$$f_T(\tau) = \lambda e^{-\lambda \cdot \tau} \quad \text{for} \quad \tau \ge 0$$
 (2.9)

So we can now express the rainfall rate R(t) as a temporal sequence of this type:

$$R(t) = \sum_{i} h_i \delta(t - t_i) \tag{2.10}$$

where $\delta(\cdot)$ is the Dirac delta function, the $\{h_i, i = 1, 2, ...\}$ are distributed according to Eq. (2.8) and are the rainfall depths and $\{t_i, i = 1, 2, ...\}$ are the corresponding rainfall instants and are computed as $t_i = t_{i-1} + \tau_i$ for i = 1, 2, ... where the $\{\tau_i\}$ are given by (2.9).

However, as we said before, not all the rain reaches the soil and is absorbed. First, we have to remove the part of rainfall intercepted by the canopy of trees and other forms of vegetation such as grass. Interception is quite complicated to model since it depends on the particular type of plant and also on the duration and intensity of the rainfall event. Here we use a very simple model: we define a threshold Δ as the quantity of rain that can be intercepted by plants so that if the depth of the rainfall event is less than Δ , no water reaches the soil and if it is greater, then Δ is subtracted from the depth of rain of that event. We can also assign different values to Δ depending on the particular type of plant, in order to include the important dependence of interception on the plant type.

Mathematically speaking, we can introduce interception in our model by simply modifying the rate λ , that tells us the frequency of rainfalls, in a way that already consider a rain with depth $h \leq \Delta$ happening with probability 0. So, the new rate will be:

$$\lambda' = \lambda \int_{\Delta}^{\infty} f_H(h)dh = \lambda e^{-\frac{\Delta}{\alpha}}$$
 (2.11)

The distribution of the rainfall depths, instead, remains unchanged even if, in principle, now the depths of an occurring rainfall event (so with $h \ge \Delta$) are reduced by Δ , namely

we have now new depths $h'_i = h_i - \Delta$. In fact, the new distribution should be

$$f_H(h') = \frac{C}{\alpha} e^{-\frac{h' + \Delta}{\alpha}}$$

where C is a normalization constant and is obtained by imposing

$$\int_{0}^{\infty} f_{H}(h')dh' = 1 \iff \frac{C}{\alpha}e^{-\frac{\Delta}{\alpha}}\int_{0}^{\infty} e^{-\frac{h'}{\alpha}}dh' = 1 \iff \frac{C}{\alpha}e^{-\frac{\Delta}{\alpha}}\alpha = 1 \iff C = e^{\frac{\Delta}{\alpha}}$$

and so

$$f_H(h') = \frac{C}{\alpha} e^{-\frac{h' + \Delta}{\alpha}} = \frac{1}{\alpha} e^{\frac{\Delta}{\alpha}} \cdot e^{-\frac{h' + \Delta}{\alpha}} = \frac{1}{\alpha} e^{-\frac{h'}{\alpha}}$$

that is the same of (2.8). So, as we said, the distributions of the new $\{h'_i\}$ and of the old $\{h_i\}$ are the same.

After these considerations, we can now group together rainfall and interception in this way:

$$R(t) - I(t) = \sum_{i} h'_{i} \delta(t - t'_{i})$$
 (2.12)

where $\{t'_i, i = 1, 2, ...\}$ are the instants of rainfall obtained as $t'_i = t'_{i-1} + \tau'_i$ and $\{\tau'_i, i = 1, 2, ...\}$ are extracted from the exponential distribution with the new rate λ' .

This is not the end of the story, in fact we still have to add the runoff contribution. The soil can absorb water up to a certain level, if the water exceeds this level, then it is converted into surface runoff. So we have to consider, in our model, an upper bound and we express it saying that the soil moisture can be at most 1.

Hence, we have to make one last modification to our distributions. First, we can normalize the mean rainfall depth α with the active soil depth, that is the height of soil in which water can be stocked and it is given by the product between the soil depth and the soil porosity, namely $n \cdot Z$. Doing this, we obtain a new dimensionless rate

$$\frac{1}{\gamma} = \frac{\alpha}{nZ} \tag{2.13}$$

Analogously, we can define normalized rainfall depths

$$y_i = \frac{h_i}{nZ}$$
 for $i = 1, 2, \dots$ (2.14)

Then, the distribution from which we extract the rainfall depths, now normalized, becomes

$$f_Y(y,s) = \gamma e^{-\gamma \cdot y} + \delta \left(y - (1-s) \right) \cdot \int_{1-s}^{\infty} \gamma e^{-\gamma \cdot u} du$$
 (2.15)

and this is valid for $0 \le y \le 1 - s$. We can see that the first term is the distribution (2.8) with the dimensionless quantity γ and y rather than α and h and has the same physical

meaning; the second term, instead, is telling us the probability that a rainfall event could produce saturation when the soil has a certain moisture s, including in this way its upper bound.

Eventually, we can now write the infiltration rate as

$$\varphi[s(t), t] = R(t) - I(t) - Q[s(t), t] = nZ \sum_{i} y_{i} \delta(t - t'_{i})$$
(2.16)

where the set of $\{y_i, i = 1, 2, ...\}$ are extracted from distribution (2.15), while $\{t'_i, i = 1, 2, ...\}$ are the same as before the considerations about runoff.

2.2.2 Losses

We can start by analyzing the evapotranspiration term which is, as we said, the sum of water evaporation from the soil and transpiration due to plants. These two phenomena are not directly related, but we can treat them together since for small values of s plants do not transpire anymore and so only evaporation remains, whereas for high values of s the main contribution is due to transpiration.

To model evapotranspiration we can assume that, as long as soil moisture is enough to let plants continue with their physiological processes without problems, the evapotranspiration rate is constant and equal to its maximum value E_{max} . Below a certain level s^* of soil moisture, then, plants begin to reduce transpiration since their stomata start to close. At this point, although complex mechanisms and processes depending on many factors come into play, we can approximate the behavior of the evapotranspiration rate as a linear one. Eventually, when soil moisture reaches the so-called wilting point s_w , the soil becomes too dry and plants start to get damaged and die. So below s_w , only evaporation remains and goes on at a very low rate until the hygroscopic point s_h is reached and the water stock in soil is not further diminished by evapotranspiration.

Hence, the functional dependence of the evapotranspiration rate is strongly non linear and follows

$$ET(s) = \begin{cases} E_w \frac{s - s_h}{s_w - s_h} & \text{for } s_h < s \le s_w \\ E_w + (E_{max} - E_w) \frac{s - s_w}{s^* - s_w} & \text{for } s_w < s \le s^* \\ E_{max} & \text{for } s^* < s \le 1 \end{cases}$$
 (2.17)

where E_{max} represents the rate of a unitary surface uniformly covered with vegetation and is a daily average of the true rate. In fact, we recall that we are not considering the dynamics of rains during a day and so, for our model, the smallest timescale is the day. We will also make the assumption that this rate remains constant during the growing seasons and, following the data provided by "Laio et al. (2001)" [5], we assign

$$E_{max}^{tree} = 0.5 \text{ cm/day}$$

for trees and

$$E_{max}^{grass} = E_{max}^{tree} - 10\% \cdot E_{max}^{tree} = 0.45 \text{ cm/day}$$

for grasses.

For the values of s^* , s_w and s_h we instead use the soil-water retention curves. As explained again in "Laio et al. (2001)" [5], those curves are in the form

$$\Psi_s = \overline{\Psi}_s \cdot s^{-b} \tag{2.18}$$

where Ψ_s is the soil matric potential, while $\overline{\Psi}_s$ and b (known as the Campbell's parameter) are experimentally determined parameters. Depending on the type of soil under consideration, very different values can be obtained for these two quantities. Then, to determine the soil-water levels s^* , s_w and s_h , we assign to the corresponding soil matric potentials, namely Ψ_{s,s^*} , Ψ_{s,s_w} and Ψ_{s,s_h} some values derived from experimental evidences and we see where these soil matric potentials intersect the soil-water retention curves, as explained in Figure 2.1. In particular, accordingly with "Laio et al. (2001)" [5], we set:

$$\Psi_{s,s^*} = -0.03 \text{ MPa}; \quad \Psi_{s,s_m} = -3 \text{ MPa}; \quad \Psi_{s,s_h} = -10 \text{ MPa}.$$

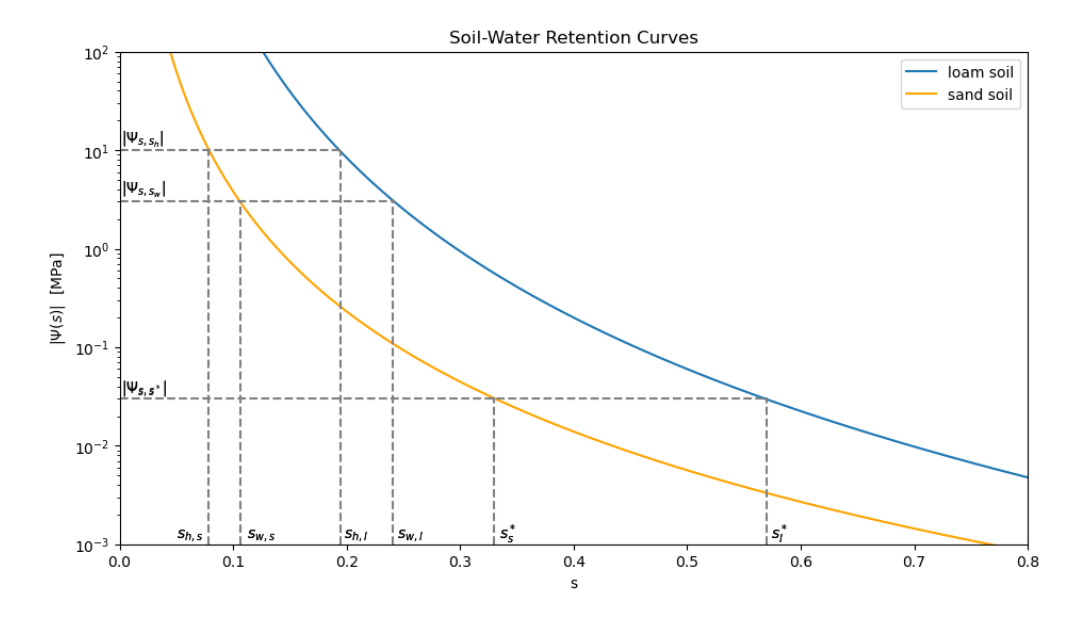


Figure 2.1. Soil-water retention curves for a loam soil (in blue) and a sand soil (in orange). To find out the values of the soil-water levels, we fix some values for the matric potential, accordingly with experimental data and independently on the soil type, and then horizontal line are drawn. The points intersected on the curves determine the soil-water levels s_h , s_w and s^* for that particular soil type. The values for some soils are reported in Table 2.1.

Finally, for the value of E_w we choose 0.01 cm/day. This is not a precise estimate, but since the losses are quite small in this part of the dynamics, a detailed analysis is not completely necessary and only the order of magnitude of E_w is really important.

Before ending the discussion about this term, we must say that our model of evapotranspiration is not completely correct for some particular ecosystems, such as extremely

	1							
	s_{ws}	s_{opt}	$\overline{\Psi}_s \ [MPa]$	$\overline{\Psi}_s$ (log) [MPa]	s_h	s_w	s^*	s_{fc}
Sand	0.11	0.19	$-1.85 \cdot 10^{-3}$	$-0.34\cdot10^{-3}$	0.08	0.11	0.33	0.35
Loamy sand	0.11	0.18	$-0.88 \cdot 10^{-3}$	$-0.17\cdot10^{-3}$	0.08	0.11	0.31	0.52
Sandy loam	0.18	0.29	$-2.10 \cdot 10^{-3}$	$-0.70\cdot10^{-3}$	0.14	0.18	0.46	0.56
Loam	0.24	0.37	$-4.68 \cdot 10^{-3}$	$-1.43 \cdot 10^{-3}$	0.19	0.24	0.57	0.65
Clay	0.53	0.64	$-3.97 \cdot 10^{-3}$	$-1.82 \cdot 10^{-3}$	0.47	0.52	0.78	≈ 1

Table 2.1. The values of s_{ws} and s_{opt} has been taken from "Bertagni et al. (2021)" [1], whereas the others come from "Laio et al. (2001)" [5].

arid habitat. In fact, in extreme situations plants may have developed different photosynthetic pathways to better adapt and, for this reason, modifications to our model have to be considered.

Now, only the leakage term remains to be modelled. For this purpose, we will assume that the leakage rate is maximum when the soil is saturated and decreases as s decreases, following the behaviour of the hydraulic conductivity K(s), so that, in practice, we set L(s) = K(s). The most common way to model the latter, is to describe this term as a power law of the form

$$K(s) = K_s \cdot s^c \tag{2.19}$$

where K_s is the saturated hydraulic conductivity, namely K(s=1), and c=2b+3 with b the same parameter as the one of Eq. (2.18).

Eventually, we can put together evapotranspiration and leakage in a unique function, normalising also the two rates by the active soil depth nZ. We get then

$$\rho(s) = \frac{ET(s) + L(s)}{nZ} = \frac{K_s}{nZ} \cdot s^{2b+3} + \begin{cases} 0 & \text{if } 0 < s \le s_h \\ \eta_w \frac{s - s_h}{s_w - s_h} & \text{if } s_h < s \le s_w \\ \eta_w + (\eta + \eta_w) \frac{s - s_w}{s^* - s_w} & \text{if } s_w < s \le s^* \\ \eta & \text{if } s^* < s \le 1 \end{cases}$$
(2.20)

where we defined

$$\eta_w = \frac{E_w}{nZ}; \quad \eta = \frac{E_{max}}{nZ}$$

This function $\rho(s)$ is a deterministic term that describes how soil moisture decays between two subsequent rainfall events. Moreover, $\rho(s)$ still has the dimension of an inverse time quantity, we will discuss how to make it dimensionless in a following section. In Figure 2.2 we report the profile of the losses term as a function of s.

Starting by Eq. (2.5) and putting all the pieces together, the differential equation

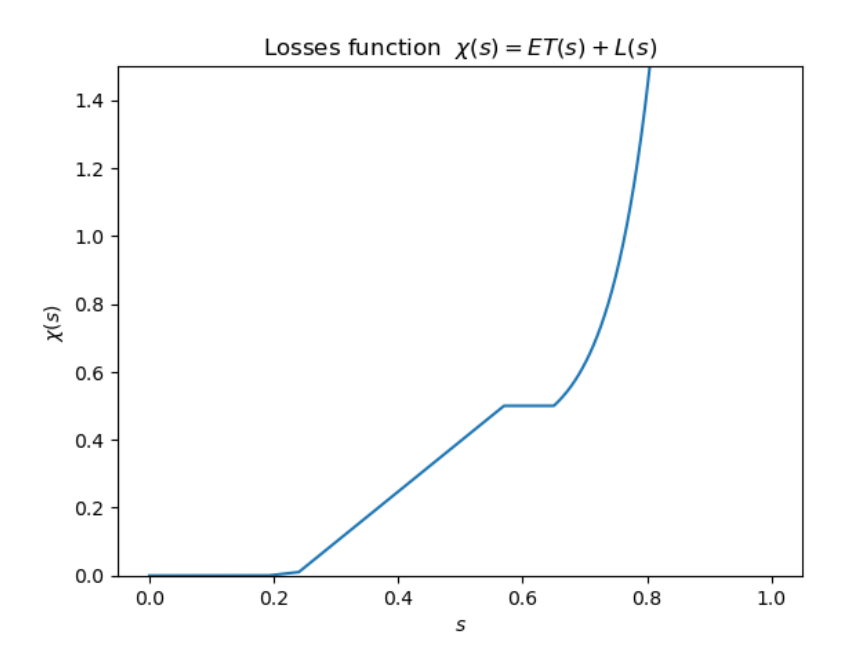


Figure 2.2. The function $\chi(s)$ which describes the losses (for a loam soil).

describing the dynamics of soil moisture now reads

$$nZ\frac{d}{dt}s(t) = \varphi[s(t), t] - \chi[s(t)] =$$

$$= nZ\sum_{i} y_{i}\delta(t - t'_{i}) - \chi(s)$$

$$\iff \frac{d}{dt}s(t) = \sum_{i} y_{i}\delta(t - t'_{i}) - \frac{\chi[s(t)]}{nZ} =$$

$$= \sum_{i} y_{i}\delta(t - t'_{i}) - \rho(s)$$

so that, in the end, we obtain:

$$\frac{d}{dt}s(t) = \sum_{i} y_i \delta(t - t_i') - \rho(s)$$
(2.21)

As an example, we report in Figure 2.3 a temporal series for the soil moisture of a loam soil.

2.3 Soil hydrogen dynamics

We can now analyse the second main equation, namely Eq. (2.4), which describes the dynamics of the hydrogen concentration in the soil. Again, for simplicity, we rename the variables \bar{c} and \bar{s} as c and s. In this equation, we have three contributions: the hydrogen

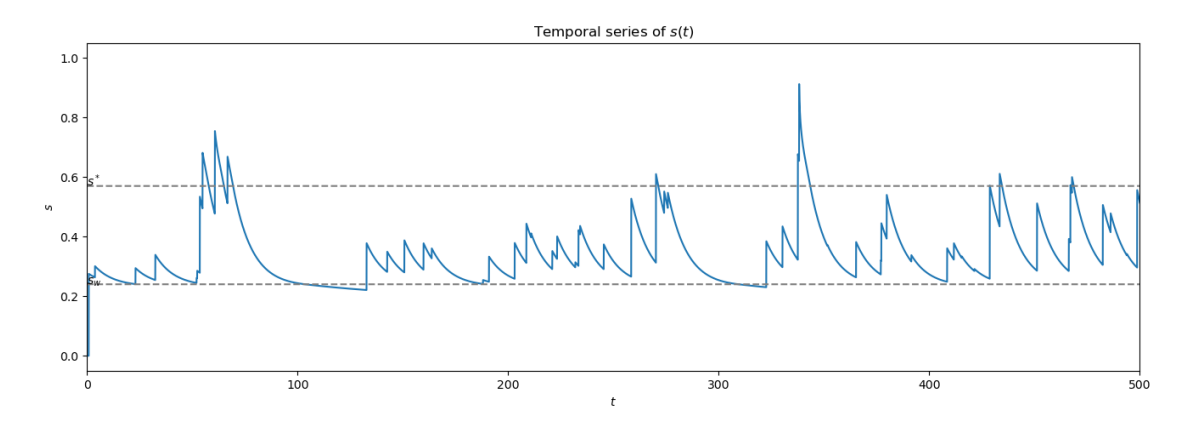


Figure 2.3. The complete dynamics of s(t) for a loam soil. The parameters used in the simulation are: Z = 30 cm, $\lambda = 0.1$ day⁻¹, $\alpha = 1.5$ cm.

flux F(s,c), the biological decay BD(s,c) of H_2 inside the soil and the soil production term P of hydrogen. We will assume the latter to be zero in the whole discussion and focus ourselves on the other two, following the reference of "Bertagni et al. (2021)" [1].

2.3.1 Atmospheric Flux of Hydrogen

In order to diffuse from the atmosphere to the soil, hydrogen may have to go through some barriers such as, for example, layers of snow or litter which may cover the soil. To keep track of those obstacles called, in general, diffusive barriers, we model them by means of an electric analogy. We define, for this purpose, a conductance of the soil g_s and a conductance of the diffusive barriers g_δ and then we compute the total one as

$$\frac{1}{g_T} = \frac{1}{g_c} + \frac{1}{g_\delta} \tag{2.22}$$

We can compute these two conductances by assuming that the dominant contribution is given by molecular diffusion, hence using the relations

$$g_c = \frac{D_c(s)}{l}; \quad g_\delta = \frac{D_\delta}{\delta}$$

where l is the length-scale of the soil diffusive layer and, experimentally, its value is $l \approx 1$ cm, while δ is the depth of the diffusive barriers, again in centimeters. D_c and D_{δ} are, instead, the diffusivities and, following "Mondrup et al. (2013)" [6], they can be computed by means of

$$\frac{D_c}{D_0} = \alpha_1 n^{\alpha_2} (1 - s)^{\alpha_3} \tag{2.23}$$

where D_0 is the H_2 diffusion coefficient in air and is estimated by "Yonemure, Yokozawa at al. (2000)" [11] to be $D_0 = 0.611 \text{ cm}^2/\text{s}$ and the α_i are parameters which depend on the model. In the following, we will use the ones of "Moldrup et al. (1999)" [7] and, for this reason, we choose $\alpha_1 = 1$, $\alpha_2 = 2$, $\alpha_3 = 2 + \frac{3}{b}$ with b the Campbell's parameter (the

same used in Eq. (2.18)). To compute D_{δ} , we may again use Eq. (2.23) setting n = 0.5 and s = 0, unless some experimentally determined values are available. We report in Figure 2.4 the profile of the total conductance for two different values of the depth of the diffusive barrier.

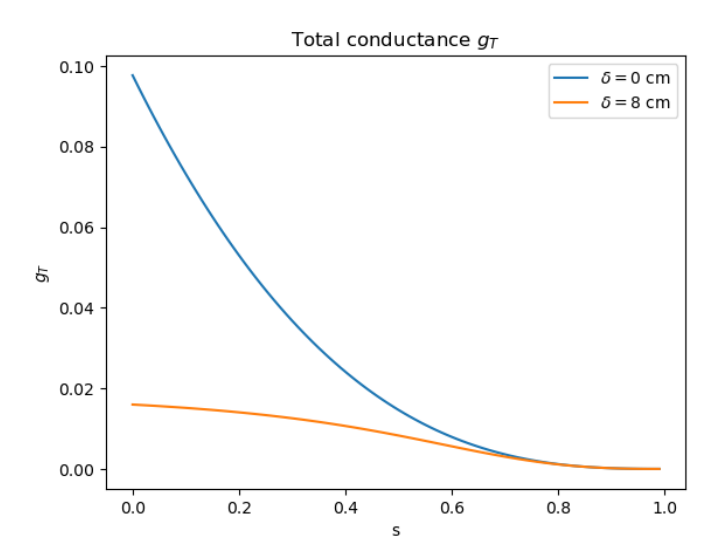


Figure 2.4. In the figure above, the total conductance for a sand soil is reported for two different depths δ of the diffusive barriers.

After these considerations, we can model the flux term as

$$F(s,c) = g_T(c_a - c) \tag{2.24}$$

where g_T is the total conductance computed as above and c_a is the atmospheric concentration of H_2 , that is, 530 ppb. We notice that the flux becomes zero whether $c = c_a$ as the soil concentration of H_2 equals the atmospheric one or when $g_T = 0 \implies D_c = 0 \implies s = 1$, namely when the soil is saturated and all the pores are already filled by water, resulting in no space left for the hydrogen to diffuse.

2.3.2 Biological Decay

The consumption of H_2 in the soil is mainly due to some bacteria whose activity depends on many factors such as temperature, type and moisture of the soil, pH, organic content and salinity. Here, as done in "Bertagni et al. (2021)" [1], we will take into account only the effects of temperature and soil moisture and neglect the others. Hence, we write the biological decay term as

$$BD(s,c,T) = k_m h(T) f(s) c (2.25)$$

where $k_m = 0.03 \text{ s}^{-1}$ is the rate at which H_2 is removed in non-limited conditions; the limitations, instead, are modeled through f(s) and h(T) which are normalized functions taking values only between 0 and 1 and describing how, respectively, soil moisture and temperature influence and limit the process. Temperature is a key factor and it has been

experimentally noticed that a maximum in the biological activity is reached between 30 °C and 40 °C, while, for colder and hotter temperatures, the bacteria metabolism decreases significantly. The fitting function that we will use for h(T) is, then, the one proposed by "Ehhalt and Rohrer (2011)" [4] and takes the form

$$h(T) = \frac{1}{1 + e^{-(T - 3.8)/6.7}} + \frac{1}{1 + e^{(T - 62.2)/7.1}} - 1.$$
 (2.26)

Its profile is shown in Figure 2.5.

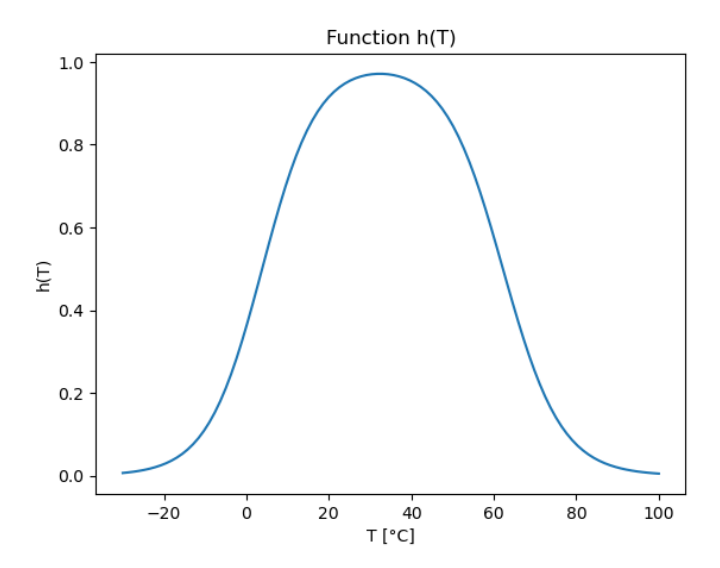


Figure 2.5. In this plot, one can see the profile of the function h(T). A maximum is obtained for a temperature around 30 °C, so that here we have the optimal temperature for the hydrogen-based metabolism of bacteria in soil. For cold and hot temperature, instead, this function describes the sudden drop in the metabolic activities by quickly tending to zero.

In f(s), instead, we include the two extreme situations: if there is little water in the soil, then bacteria's metabolism is reduced considerably, to the point that they enter a state called dormancy, and therefore the hydrogen consumption drops. However, even if the soil moisture is too high, the biological decay becomes zero. Experimentally, in fact, it seems that the biological processes of the soil bacteria are also hindered in this condition, although the physical and chemical mechanisms behind this phenomenon are not yet fully understood. This means that, between these two opposite situations, there must be a value of soil moisture s_{opt} that maximizes the metabolic activity of the bacteria. To model the function f(s) keeping track of the previous consideration, a family of modified beta distributions is used, so that

$$f(s) = \frac{1}{N}(s - s_{ws})^{\beta_1}(s_{up} - s)^{\beta_2}$$
(2.27)

in which N is a normalization constant defined in order to get max(f) = 1 and the beta parameters are set equal to $\beta_1 = 0.4$ and $\beta_2 = \beta_1 \frac{(1-s_{opt})}{(s_{opt}-s_{ws})}$ to ensure that the maximum

of f(s) is reached for $s=s_{opt}$. Finally, in the relation above, we define s_{up} and s_{ws} as, respectively, the upper and lower values of soil moisture among which the bacteria's metabolism works. To estimate those two values and also s_{opt} , we again use the soil-water retention curves, namely Eq. (2.18), introducing a soil matric potential for each of these levels of soil moisture and seeing where they cross the curves. We stress once more that these curves and, consequently, the soil moisture levels strongly depend on the soil type under study. For the numerical values, we follow "Smith-Downey et al. (2006)" [10] and "Conrad and Seiler (1981)" [2], in particular setting $s_{up} = 1$, which means that there are no limitations for the decrease of the air volume in soil, unless we reach the saturation condition for the soil moisture. The values of s_{sw} and s_{opt} for some soils are instead reported in Table 2.1. In Figure 2.6, the profile of f(s) is shown for two different soil types.

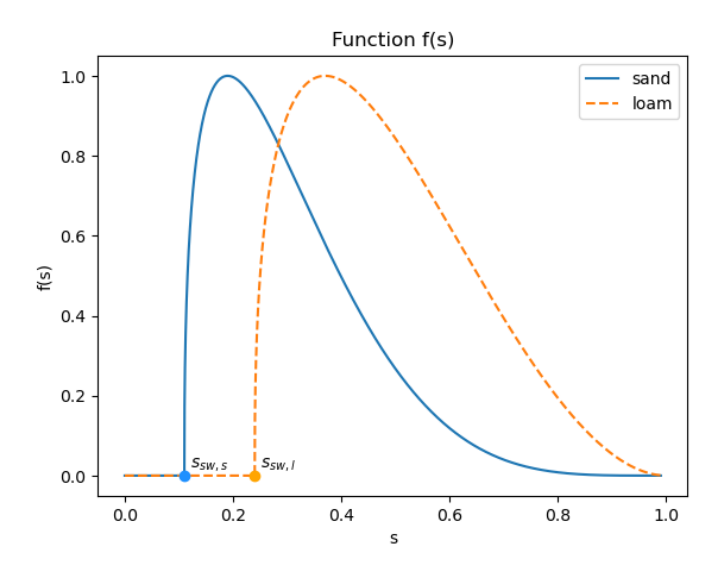


Figure 2.6. The function f(s) for two different soil types: a sand soil in blue and a loam soil in orange. We can see that below s_{ws} and above $s_{up} = 1$ this functions drop to zero as the bacteria metabolism stops to work.

2.4 Simulations and results of the model

2.4.1 Quasi-steady state approximation

Now that we have modeled the two main equations, we can simulate them both by fixing the temperature and the depth of the diffusive barriers in order to keep only s and c as variables. An example of such a simulation is given in Figure 2.7 (a). We notice how the H_2 dynamics is strongly influenced by that of the soil moisture, especially when a rain event occurs and s(t) suddenly increases, producing, as a consequence, a sharp drop of the hydrogen concentration in the soil. Moreover, c(t) reaches the atmospheric level $c_a = 530$ ppb each time s(t) goes below s_{ws} , which we recall from the previous section

to be the lowest value of s after which bacterial metabolism stops working. Without being depleted by soil bacteria and with poor water to hinder its diffusion, the hydrogen concentration can, thus, reach its maximum value until the next rain event occurs.

We can also see that the two actors, F(s,c) and BD(s,c), involved in the hydrogen dynamics are equal for each time, namely $F=Z\cdot BD$, as shown in Figure 2.7 (b). This means that in Eq. (2.4) the time derivative of c is negligible, as if the H_2 dynamics were in a quasi-steady state regime. This is not completely surprising: one may have noticed, in fact, that all the time units of the quantity related to the soil moisture dynamics are expressed in days, whereas those describing the H_2 dynamics are in seconds. The two equations have, hence, different time scales and the hydrogen dynamics is much faster than the other. Therefore, c adapts quite instantly to the time variations of s and this is the reason why, mathematically, we may neglect the left side of Eq. (2.4). From these considerations, we can obtain an analytical relationship to directly compute c:

$$nZ\frac{d}{dt}[(1-s)c] = 0 = F - Z \cdot BD \iff$$

$$\iff F = Z \cdot BD \iff$$

$$\iff g_T(c_a - c) = Zk_mh(T)f(s)c \iff$$

$$\iff c \cdot [g_T + Zk_mh(T)f(s)] = g_Tc_a \iff$$

$$\iff c = \frac{c_a}{1 + \frac{Zk_mh(T)f(s)}{g_T}}$$

We may call $v_{BD} = Zk_mh(T)f(s)$ since, dimensionally, this quantity is a velocity. It is also useful to define this quantity, since it sums up all the terms which describe the biological sink of H_2 . So, finally, we get

$$c_{qss}(t) = \frac{c_a}{1 + \frac{v_{BD}}{q_T}} \tag{2.28}$$

where with the notation c_{qss} we mean the hydrogen concentration in soil in the quasi steady-state approximation.

In Figure 2.8, we plot both the numerical solution for c obtained from Eq. (2.4) and the analytical form of c just derived in Eq. (2.28). One can see that the two profiles superimpose perfectly, telling us that the quasi-steady state approximation for the hydrogen dynamics is very reasonable.

2.4.2 Deposition velocity and limitations

At this point, we can define the key quantity that tells us how the hydrogen uptake process is influenced by the various factors. This is the deposition velocity v_d and its definition is the following

$$v_d = \frac{F}{c_a}$$

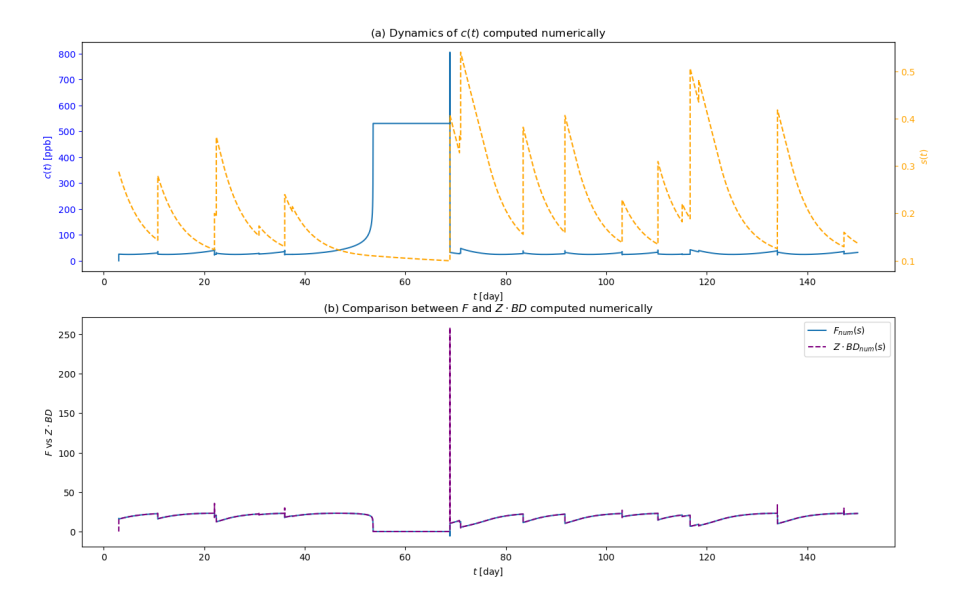


Figure 2.7. The coupled dynamics of s(t) and c(t) is reported in (a), while the comparison between the flux term F(t) and the biological decay term BD(t) is shown in (b). Both are computed solving numerically equations (2.21) and (2.4) for a loamy sand soil. The simulation's parameters are: $Z=30~cm,~\lambda=0.2~day^{-1},~\alpha=1.5~cm,~T=20^{\circ}C$ and $\delta=1~cm$.

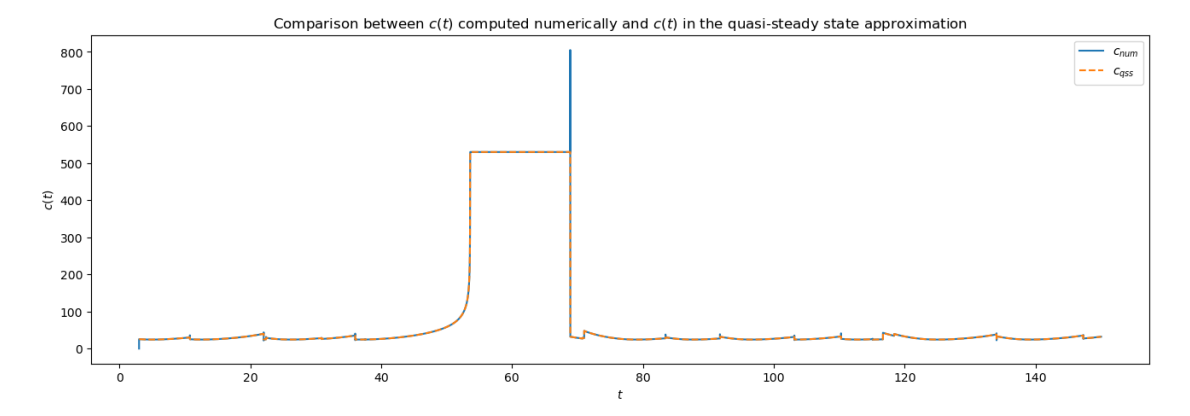


Figure 2.8. The comparison between the numerical solution of Eq. (2.4) and the analytical form of Eq. (2.28) obtained using the quasi-steady state approximation. The two profiles superimpose quite perfectly. The parameters used are the same of Figure 2.7.

In order to obtain an analytical relation also for v_d , we can compute the flux term F using for c the quasi-steady state approximation, namely Eq. (2.28), so that we get

$$\begin{aligned} v_d &= \frac{F}{c_a} = \\ &= \frac{g_T(c_a - c_{qss})}{c_a} = \\ &= \frac{g_T\left(c_a - \frac{g_Tc_a}{18^{g_T + v_{BD}}}\right)}{c_a} = \\ &= \frac{g_Tc_a\left(1 - \frac{g_T}{g_T + v_{BD}}\right)}{c_a} = \\ &= \frac{g_T \cdot v_{BD}}{g_T + v_{BD}} \end{aligned}$$

Eventually, we obtain the relation

$$v_d(t) = \frac{g_T \cdot v_{BD}}{g_T + v_{BD}} \tag{2.29}$$

In Figure 2.9, we plot v_d as a function of temperature and soil moisture for different soil types. One can see that for $s < s_{ws}$ we have $v_d = 0$. This is because, below s_{ws} , the biological decay drops to zero since bacteria enter the inactive state and, consequently, $v_{BD} = 0$, which means that no hydrogen is absorbed. Then, for values of s slightly above s_{ws} , bacteria become active and the diffusion of H_2 into the soil is maximized, hence we have here the highest values of hydrogen uptake and, thus, of v_d . In particular, the maxima are reached when the temperature is also optimal, namely, as we said before, between 30 °C and 40 °C. Finally, for higher s, we said that hydrogen diffusion is hindered and, for this reason, the deposition velocity decreases until it reaches again the zero value when the soil is saturated, that is, when s = 1. In "Bertagni et al. (2021)" [1], some comparisons with experimental data are reported and one can see how our model fits them well. Moreover, with these experiments the role of the diffusive barriers is also investigated and one can see how much hydrogen uptake diminishes when the soil is, for example, covered with snow.

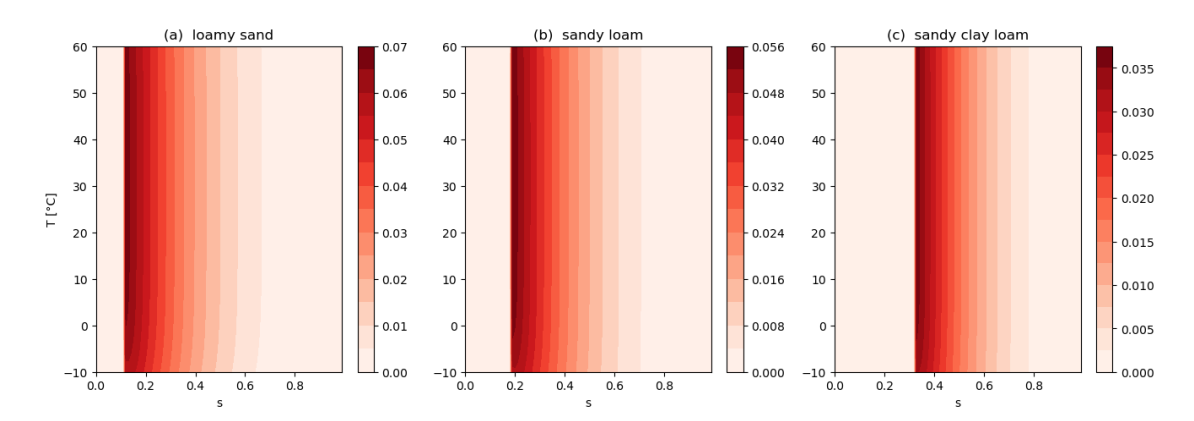


Figure 2.9. The deposition velocity as a function of T and s for three different soil types and with parameters $\delta=0$ cm and Z=15 cm.

All these discussions make us understand the crucial role of v_d . In fact, we have seen that there are two main limitations to the hydrogen uptake: the biotic one, namely the fact that bacteria metabolism stops working if the soil is too dry, and the diffusive limitation, that is, when the soil is so moist that hydrogen diffusion into soil proceeds with difficulty. Mathematically speaking, the first limitation is encoded in the v_{BD} term, while the latter is described by g_T . One can see that v_d is half the harmonic mean of these two terms and, for this reason, it is quite easy to verify which of the two limitations is acting in a possible experimental situation: if we are in a case in which the dominant limitation is the diffusive one, then it means that $g_T << v_{BD}$ and, consequently, $v_d \sim g_T$. Instead, if we are in the opposite situation and the biotic limitation dominates, then

 $g_T >> v_{BD}$, which implies $v_d \sim v_{BD}$. Hence, we can summarize by saying

$$v_d \sim \begin{cases} g_T & \text{if } g_T << v_{BD} \text{ (diffusive limitation)} \\ v_{BD} & \text{if } g_T >> v_{BD} \text{ (biotic limitation)} \end{cases}$$
 (2.30)

To better understand these points, we show in Figure 2.10 v_d , g_T and v_{BD} in three possible atmospheric conditions: two cold climates with and without snow and a temperate climate. In these plots, we can see how the two limitations act on v_d as s varies. For low values of s, as we said, the biotic limitation dominates and v_d follows the profile of v_{BD} . This occurs in arid regions and during the dry season of zones with a tropical savanna climate. Instead, for higher values of soil moisture, the diffusive limitation takes over. This is typical of temperate and tropical humid regions and also of the wet season of zones with a tropical savanna climate.

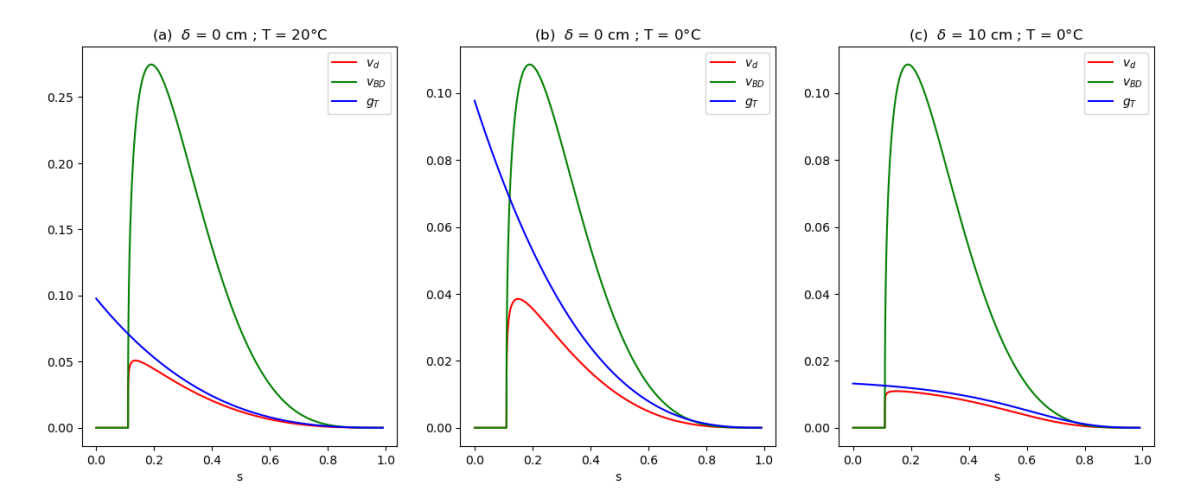


Figure 2.10. The function v_d , g_T and v_{BD} for a sand soil in three different climate: in (a) a temperate climate is reproduce with a temperature of T = 20 °C and no diffusive barriers; in (b) we have the case of a cold soil with T = 0 °C but without diffusive barriers (no snow); in (c) is plotted a cold climate with also the presence of a diffusive barrier, such as snow.

Eventually, for colder regions such as cold humid climates, also the temperature starts to play a role in the reduction of the hydrogen uptake. Here, in fact, both biotic and diffusive factors hinder the process. In particular, if there is no snow cover on the soil, g_T and v_{BD} are comparable and none of them dominates the other. However, if the presence of a snow cover is taken into account, again the H_2 uptake becomes a diffusive limited process.

So, as we saw, measuring v_d can be a simple way to summarize well how the hydrogen uptake is influenced by all those factors. Moreover, we briefly analyzed how our model changes on the macroscopic scale. In the following sections, we are going to describe what happens if we keep also the dependencies on the spatial dimensions (which we neglected in the beginning), namely we will consider s and s depending on s and s are s and s

investigate how the local dynamics inside the same ecosystem changes due to spatial inhomogeneities.

Chapter 3

Space-Dependent Dynamics

3.1 Integrating horizontal diffusion processes

In this chapter, our aim is to introduce the horizontal spatial dependencies in the equations and to investigate their effects on our model. As a consequence, another physical phenomenon has to be taken into account: spatial diffusion, both of moisture and hydrogen. Until now, the two equations under study have been

$$\frac{\partial}{\partial t}s(t) = \sum_{i} [y_i \delta(t - t_i')] - \rho(s(t))$$

$$nZ_r \cdot \frac{\partial}{\partial t}[(1 - s(t)) \cdot c(t)] = F(s, c) - Z_r \cdot BD(s, c)$$

Instead, by including spatial dependencies and horizontal diffusion processes, they become

$$\frac{\partial}{\partial t}s(t,\vec{x}) = \sum_{i} [y_i \delta(t - t_i')] - \rho(s(t,\vec{x})) + \vec{\nabla} \cdot [D_s \vec{\nabla} s(t,\vec{x})]$$
(3.1)

and

$$nZ_r \cdot \frac{\partial}{\partial t} [(1 - s(t, \vec{x})) \cdot c(t, \vec{x})] = F(s, c) - Z_r \cdot BD(s, c) + \vec{\nabla} \cdot [D_c \vec{\nabla} c(t, \vec{x})]$$
(3.2)

where D_s and D_c are the two diffusion coefficients, respectively, of s and c. We have not explicit the dot product since, in principle, these two quantities could depend on spatial variables. Indeed, we have already encountered D_c in the modelling of the F(s,c) term, which describes the atmospheric flux of hydrogen. In that context, we defined a diffusion coefficient for the hydrogen and we adopted the formula (2.23) from "Mondrup et al. (1999)" [7]. One can see that D_c depends on the spatial variables through s and hence it is, for sure, not constant. We will use here the same model for D_c .

For the other diffusion coefficient, namely for D_s , we will start, for simplicity, by considering it constant and then we will make a more realistic hypothesis for its model and use a non-linear version.

3.2 Analysis of possible Turing instabilities

Before going on with the modelling of our equations, we have to consider some of the possible physical effects that diffusion processes can bring about. In particular, we can now ask ourselves: could this model show Turing-like instabilities?

This particular type of instabilities can take place in a reaction-diffusion system, that is, a system in which components can react between themselves and diffuse. Under certain conditions, the combination of these two processes can produce a steady state which is heterogeneous and shows spatial patterns: the so-called Turing instabilities. Their peculiarity is that they are induced by diffusion: without this process, the system would reach a steady state spatially homogeneous and stable to small perturbations. This could be counterintuitive since, generally, diffusion is the process that tends to smooth spatial heterogeneous regions over time to reach a steady state that is homogeneous. However, as we said, sometimes the opposite happens, but only if specific conditions are satisfied and we will see and analyse later which they are.

The mathematical form of a reaction-diffusion system (with only two reactants as in our case) is:

$$\begin{cases} \frac{\partial u}{\partial t} = f(u, v) + D_u \nabla^2 u \\ \frac{\partial v}{\partial t} = g(u, v) + D_v \nabla^2 v \end{cases}$$
(3.3)

where u and v are the two reactants, $f(\cdot)$ and $g(\cdot)$ the functions describing the reaction terms, D_u and D_v the diffusion coefficients.

Going back to our model and assuming that both D_s and D_c are constants, we see that Eq. (3.1) is already in the form of a reaction-diffusion equation, while Eq. (3.2) needs some manipulations. Moreover, eq. (3.2) is not completely correct: we add the diffusion term before making the time derivative of c(t,x) explicit and, hence, the dimensions of the various terms are not all equal. Therefore, we rewrite it following these naive steps: first $\frac{dc}{dt}$ must be isolated

$$nZ_r \cdot \frac{d[(1-s)c]}{dt} = F - Z_r \cdot BD \iff$$

$$\iff (1-s)\frac{dc}{dt} - c\frac{ds}{dt} = \frac{F - Z_r \cdot BD}{nZ_r} \iff$$

$$\iff \frac{dc}{dt} = \frac{1}{1-s} \left[\frac{F - Z_r \cdot BD}{nZ_r} + c\frac{ds}{dt} \right]$$

and then we add the diffusion term (considering, as we said, a constant diffusion coefficient), obtaining

$$\frac{\partial c}{\partial t} = \frac{1}{1 - s} \left[\frac{F - Z_r \cdot BD}{nZ_r} + c \frac{\partial s}{\partial t} \right] + D_c \nabla^2 c \tag{3.4}$$

Indeed, our model is now in the form of a reaction-diffusion system and we can write it as

$$\begin{cases} \frac{\partial s}{\partial t} = S(t,s) + D_s \nabla_x^2 s \\ \frac{\partial c}{\partial t} = C(t,s,c) + D_c \nabla_x^2 c \end{cases}$$
(3.5)

where we define

$$S(t,s) = \sum_{i} (y_i \delta(t - t_i')) - \rho(s)$$

and

$$C(t, s, c) = \frac{1}{1 - s} \left[\frac{F - Z_r \cdot BD}{nZ_r} + c \cdot \left(\sum_i y_i \delta(t - t_i') - \rho(s) \right) \right].$$

3.2.1 Dimensionless equations

To verify whether Turing instabilities can take place or not, it is convenient first to make our equations dimensionless. In order to do so, we define:

$$\tilde{t} = \frac{t}{T}$$
 ; $\tilde{x} = \frac{x}{\sqrt{D_s \cdot T}} \iff t = T \cdot \tilde{t}$; $x = \tilde{x}\sqrt{D_s \cdot T}$

introducing two new dimensionless variables, \tilde{t} and \tilde{x} , and a new parameter T that represents a certain physically meaningful time scale. When these two variables are substituted into the first equation (the one describing the dynamics of s(t,x)) one gets:

$$\frac{\partial s}{\partial t} = \sum_{i} (y_{i}\delta(t - t'_{i})) - \rho(s) + D_{s}\nabla_{x}^{2}s \iff$$

$$\iff \frac{1}{T}\frac{\partial s}{\partial \tilde{t}} = \sum_{i} y_{i}\delta(T \cdot \tilde{t} - t'_{i}) - \rho(s) + \frac{D_{s}}{T \cdot D_{s}}\nabla_{\tilde{x}}^{2}s \iff$$

$$\iff \frac{1}{T}\frac{\partial s}{\partial \tilde{t}} = \sum_{i} y_{i}\delta\left(T\left(\tilde{t} - \frac{t'_{i}}{T}\right)\right) - \rho(s) + \frac{1}{T}\nabla_{\tilde{x}}^{2}s$$

exploiting the property of the Dirac delta functions that tells $\delta(ax) = \frac{1}{|a|}\delta(x)$ one obtains

$$\frac{1}{T}\frac{\partial s}{\partial \tilde{t}} = \sum_{i} \frac{y_{i}}{T} \delta\left(\tilde{t} - \frac{t_{i}'}{T}\right) - \rho(s) + \frac{1}{T} \nabla_{\tilde{x}}^{2} s$$

we can now multiply each term by the time scale T

$$\frac{\partial s}{\partial \tilde{t}} = \sum_{i} y_{i} \delta \left(\tilde{t} - \frac{t'_{i}}{T} \right) - T \cdot \rho(s) + \nabla_{\tilde{x}}^{2} s$$

and define $\tilde{t}_i' = \frac{t_i'}{T}$ and $\tilde{\rho}(s) = T \cdot \rho(s)$ to get eventually

$$\frac{\partial s}{\partial \tilde{t}} = \sum_{i} y_{i} \delta \left(\tilde{t} - \tilde{t}'_{i} \right) - \tilde{\rho}(s) + \nabla_{\tilde{x}}^{2} s \tag{3.6}$$

where each term is now dimensionless. In fact, the dimension of $\rho(s)$ is an inverse time, while s and the $\{y_i\}$ are already non-dimensional. As a remark, we could use the time

scale T to redefine a whole set of new dimensionless parameters inside $\rho(s)$, which we remember to be in the form of Eq. (2.20). In particular, we get

$$\tilde{\rho}(s) = T \cdot \rho(s) = \frac{T \cdot K_s}{nZ_r} \cdot s^{2b+3} + \begin{cases} 0 & \text{if } 0 < s \le s_h \\ T\eta_w \frac{s - s_w}{s_w - s_h} & \text{if } s_h < s \le s_w \\ T\eta_w + T(\eta - \eta_w) \frac{s - s_w}{s^* - s_w} & \text{if } s_w < s \le s^* \\ T\eta & \text{if } s^* < s \le 1 \end{cases}$$

and by introducing the new set of normalised parameters

$$\tilde{\eta}_w = T \cdot \eta = \frac{T \cdot E_w}{nZ_r} \quad ; \quad \tilde{\eta} = T \cdot \eta = \frac{T \cdot E_{max}}{nZ_r} \quad ; \quad \tilde{K}_s = \frac{T \cdot K_s}{nZ_r}$$

we obtain

$$\tilde{\rho}(s) = \tilde{K}_{s} \cdot s^{2b+3} + \begin{cases} 0 & \text{if } 0 < s \leq s_{h} \\ \tilde{\eta}_{w} \frac{s - s_{w}}{s_{w} - s_{h}} & \text{if } s_{h} < s \leq s_{w} \\ \tilde{\eta}_{w} + (\tilde{\eta} - \tilde{\eta}_{w}) \frac{s - s_{w}}{s^{*} - s_{w}} & \text{if } s_{w} < s \leq s^{*} \\ \tilde{\eta} & \text{if } s^{*} < s \leq s_{fc} \end{cases}$$
(3.7)

Regarding the second equation, namely Eq. (3.4) which describes the hydrogen dynamics, we can proceed analogously by substituting \tilde{t} and \tilde{x} following these steps:

$$\frac{\partial c}{\partial t} = \frac{1}{1 - s} \left[\frac{F - Z_r \cdot BD}{nZ_r} + c \cdot \left(\sum_i y_i \delta(t - t_i') - \rho(s) \right) \right] + D_c \nabla_x^2 c \iff \frac{1}{T} \frac{\partial c}{\partial \tilde{t}} = \frac{1}{1 - s} \left[\frac{F - Z_r \cdot BD}{nZ_r} + c \cdot \left(\sum_i y_i \delta(T \cdot \tilde{t} - t_i') - \rho(s) \right) \right] + \frac{D_c}{T \cdot D_s} \nabla_{\tilde{x}}^2 c$$

multiplying each term by T and repeating the same considerations for the term $\sum_i y_i \delta(T \cdot \tilde{t} - t_i') - \rho(s)$ that has just been analysed, we get to

$$\frac{\partial c}{\partial \tilde{t}} = \frac{1}{1-s} \left[\frac{T \cdot (F - Z_r \cdot BD)}{nZ_r} + c \cdot \left(\sum_i y_i \delta \left(\tilde{t} - \tilde{t}_i' \right) - \tilde{\rho}(s) \right) \right] + \frac{D_c}{D_s} \nabla_{\tilde{x}}^2 c.$$

We can still define some new functions \tilde{F} and \tilde{BD} as

$$\tilde{F} = \frac{T \cdot F}{nZ_r} = \frac{TF}{nZ_r} \cdot g_t(c_a - c) = \tilde{g}_t(c_a - c)$$
 where $\tilde{g}_t = \frac{T}{nZ_r} \cdot g_t$

and

$$\tilde{BD} = \frac{T \cdot BD}{n} = \frac{T}{n} \cdot k_m \cdot h(T) \cdot f(s) \cdot c = \tilde{k}_m \cdot h(T) \cdot f(s) \cdot c \quad \text{where} \quad \tilde{k}_m = \frac{T}{n} \cdot k_m$$

in order to obtain

$$\frac{\partial c}{\partial \tilde{t}} = \frac{1}{1-s} \left[\tilde{F} - \tilde{BD} + c \cdot \left(\sum_{i} y_{i} \delta \left(\tilde{t} - \tilde{t}'_{i} \right) - \tilde{\rho}(s) \right) \right] + \frac{D_{c}}{D_{s}} \nabla_{\tilde{x}}^{2} c$$
 (3.8)

where each term is dimensionless, apart from the ones involving c which is still in the dimension of ppb.

Hence, summing up, our system, now nondimensional, is

$$\begin{cases} \frac{\partial s}{\partial \tilde{t}} = \sum_{i} y_{i} \delta\left(\tilde{t} - \tilde{t}'_{i}\right) - \tilde{\rho}(s) + \nabla_{\tilde{x}}^{2} s \\ \frac{\partial c}{\partial \tilde{t}} = \frac{1}{1 - s} \left[\tilde{F} - \tilde{BD} + c \cdot \left(\sum_{i} y_{i} \delta\left(\tilde{t} - \tilde{t}'_{i}\right) - \tilde{\rho}(s)\right)\right] + \frac{D_{c}}{D_{s}} \nabla_{\tilde{x}}^{2} c \end{cases}$$

which we can eventually rewrite in the general form

$$\begin{cases} \frac{\partial s}{\partial \tilde{t}} = f(t,s) + \nabla_{\tilde{x}}^2 s \\ \frac{\partial c}{\partial \tilde{t}} = g(t,s,c) + d \cdot \nabla_{\tilde{x}}^2 c \end{cases}$$
(3.9)

where we define

•
$$f(t,s) = \sum_{i} y_{i} \delta\left(\tilde{t} - \tilde{t}'_{i}\right) - \tilde{\rho}(s)$$

•
$$g(t, s, c) = \frac{1}{1 - s} \left[\tilde{F}(s, c) - \tilde{BD}(s, c) + c \cdot \left(\sum_{i} y_{i} \delta \left(\tilde{t} - \tilde{t}'_{i} \right) - \tilde{\rho}(s) \right) \right]$$

•
$$d = \frac{D_c}{D_s}$$

3.2.2 Conditions for the validity of Turing instabilities

Now that our model is in the form of a non-dimensional reaction diffusion system, we will try to verify whether it could show Turing instabilities or not. How to do so is explained in a detailed manner in a number of books, as an example we cite here "Mathematical Biology" by J. D. Murray [9]. Summing up, given a generic system such as

$$\begin{cases} \frac{\partial u}{\partial t} = f(u, v) + \nabla^2 u \\ \frac{\partial v}{\partial t} = g(u, v) + d \cdot \nabla^2 v \end{cases}$$
(3.10)

it must satisfy the following four conditions:

1.
$$f_u + g_v < 0$$

$$2. f_u \cdot g_v - f_v \cdot g_u > 0$$

3.
$$d \cdot f_u + q_v > 0$$

4.
$$(d \cdot f_u + g_v)^2 - 4d \cdot (f_u \cdot g_v - f_v \cdot g_u) > 0$$

Where, for the sake of clarity, f_u stands for $\frac{\partial f}{\partial u}$, while f_v means $\frac{\partial f}{\partial v}$ and so on. Combining the first with the third, one gets

$$\begin{cases} f_u + g_v < 0 \\ d \cdot f_u + g_v > 0 \end{cases} \iff \begin{cases} g_v < -f_u \\ g_v > -d \cdot f_u \end{cases}$$

ending up to the general condition

$$-d \cdot f_u < g_v < -f_u. \tag{3.11}$$

This relation tells us two things: firstly d, that is the ratio between the two diffusion coefficients, must be necessarily different from 1, namely $d \neq 1$, and secondly that the two partial derivatives f_u and g_v must have opposite signs. Indeed, if, for example, we suppose $f_u > 0$ then g_v will have to be less than 0, that is, $g_v < 0$, otherwise, according to (3.11), a positive number should be included between two negative numbers, which is impossible. Analogously, if we consider $f_u < 0$, then $g_v > 0$ otherwise a negative number should be included between two positive ones, which is, again, impossible. Therefore, as we said, f_u and g_v must have opposite signs. We underline that these conditions must be true for any general system to exhibit Turing instabilities.

For our particular model, namely (3.9), f_v can be easily computed, remembering that for us $u \equiv s$ and $v \equiv c$, and one gets

$$f_v \equiv f_c = \frac{\partial f}{\partial c} = 0$$

So, if we now analyse the condition 2 for having Turing instabilities, we obtain

$$f_u \cdot g_v - f_v \cdot g_u > 0 \iff$$

$$\iff f_s \cdot g_c - f_c \cdot g_s > 0 \iff$$

$$\iff f_s \cdot g_c - 0 > 0 \iff$$

$$\iff f_s \cdot g_c > 0$$

hence, condition 2 for our system implies that $f_u \equiv f_s$ and $g_v \equiv g_c$ should have the same sign. However, this is in contradiction with the general relation (3.11). Therefore, our system (3.9) cannot simultaneously satisfy all four conditions for Turing instabilities.

This result, which has been mathematically proven, was actually expected: our system has a particularity, that is, the two equations are coupled only in one direction. In fact, the dynamics of the hydrogen concentration c is influenced by the one of s, however the vice versa is not true and the temporal and spatial evolution of the soil moisture s is completely independent from c. This interconnection between s and c is a fundamental physical ingredient for the Turing instabilities to be shown, and, without it, a system cannot exhibit these particular types of spatial patterns.

3.3 1D model

After having understood that Turing-like instabilities cannot appear in our model, we proceed now with the investigation on the effects of a dimensionality D that is $D \ge 1$. In particular, in this section we will study the D = 1 case. The equations (3.1) and (3.4) hence become

$$\begin{cases}
\frac{\partial}{\partial t}s(t,x) = \sum_{i} \left[y_{i}\delta(t-t_{i})\right] - \rho(s) + \frac{\partial}{\partial x}\left(D_{s}\frac{\partial s(t,x)}{\partial x}\right) \\
\frac{\partial}{\partial t}c(t,x) = \frac{1}{1-s(t,x)}\left[\frac{F-Z_{r}\cdot BD}{nZ_{r}} + c(t,x)\frac{\partial s(t,x)}{\partial t}\right] + \frac{\partial}{\partial x}\left(D_{c}\frac{\partial c(t,x)}{\partial x}\right)
\end{cases} (3.12)$$

As we said at the beginning of this chapter, the hydrogen diffusion coefficient is not constant since it is equal to (2.23), therefore the second equation can be rewritten by exploiting the dot product and one gets

$$\frac{\partial}{\partial t}c(t,x) = \frac{1}{1-s} \left[\frac{F - Z_r \cdot BD}{nZ_r} + c \frac{\partial s}{\partial t} \right] + D_c' \frac{\partial s}{\partial x} \frac{\partial c}{\partial x} + D_c \frac{\partial^2}{\partial x^2} c$$
 (3.13)

where D'_c stands for the derivative of D_c with respect to s and is equal to

$$D_c'(s) = \frac{dD_c(s)}{ds} = -D_0 \alpha_1 n^{\alpha_2} \alpha_3 (1-s)^{\alpha_3 - 1}.$$
 (3.14)

Regarding the other diffusion coefficient, namely D_s , we will start by investigating what happens to our model if D_s is kept constant, and, later, the effects on our equations of a non-linear D_s will be analysed.

3.3.1 Quasi-Steady State Approximation

Before continuing with the solutions and results of the 1D model, a remark must be made: the following simulations and plots have been obtained not using the complete equation for the hydrogen dynamics, namely eq. (3.13), but its quasi-steady state approximation. In fact, as we already mentioned, the two equations in (3.12) have different time scales: the one describing the dynamics of s(t,x) has a time scale of the days, while the other evolves on the time scale of the seconds. This difference is easy to be solved analytically, however it is not numerically and makes our simulations really long. Therefore, to obtain simulations long enough to make averages, but still runnable in a few minutes, we will not use eq. (3.13) but its quasi-steady state version, which we are going to derive in a moment. We already shown that in the 0-dimensional model the solutions obtained from the two equations superimpose quite perfectly (Figure (2.8)), we will make an analogous comparison at the end of this section for much shorter simulations in order to prove that the approximation is still valid in D = 1.

Hence, to obtain the quasi-steady state approximation the idea is the same as in the 0-dimensional case: we set

$$\frac{\partial}{\partial t} \to 0$$

so that, equation (3.13) becomes

$$0 = \frac{1}{1-s} \left[\frac{F - Z_r \cdot BD}{nZ_r} + 0 \right] + D_c' \frac{\partial s}{\partial x} \frac{\partial c}{\partial x} + D_c \frac{\partial^2}{\partial x^2} c \iff \frac{\partial^2}{\partial x^2} c + \frac{D_c'}{D_c} \frac{\partial s}{\partial x} \frac{\partial c}{\partial x} = -\frac{1}{nZ_r (1-s)D_c} [F(s,c) - Z_r \cdot BD(s,c)]$$

This equation is now a second order differential equation with respect to the space variable, namely a Poisson-like equation. It can be solved with a number of different methods; we have used here an implicit one based on finite-differences following, for example, the procedure in "Nagel et al. (2014)" [8]. All the passages for our case are reported in Appendix A.

3.3.2 Cases with a constant D_s

In this first analysis of the solutions to the 1D model, the equations that we will consider are: eq. (3.13) for the dynamics of c(t, x), but in the quasi steady-state approximation; while for the dynamics of s(t, x) we will use the first of the two equations in (3.12) but with a constant D_s , so that it becomes:

$$\frac{\partial}{\partial t}s(t,x) = \sum_{i} \left[y_i \delta(t-t_i) \right] - \rho(s) + D_s \frac{\partial^2 s(t,x)}{\partial x^2}. \tag{3.15}$$

Firstly, a plot of the homogeneous case is shown in Figure 3.1 for a soil of type loam. In this situation, the diffusion processes in both the profiles of s(t,x) and c(t,x) do not play any role. In fact, since no heterogeneity of any kind has been inserted, there are no spatial gradients and the diffusion does not enter in action. Only changes due to the temporal evolution caused by rain events and their consequent drying off are visible in the profiles of s(t,x) and c(t,x).

In order to see the effects of diffusion processes, a non homogeneous initial condition is chosen, that is, the soil starts the simulation with a moisture equal to

$$s_0(x) = \begin{cases} 0.6 & \text{if } 50 \text{ cm} < x \le 150 \text{ cm} \\ 0.4 & \text{otherwise} \end{cases}$$
 (3.16)

One can see, especially in the deterministic simulations of Figure 3.2, how the diffusion of both s(t,x) and c(t,x) is now evident and smooths their spatial profiles over time until homogeneous ones are reached. Also in the plots in which rain events are considered, the diffusion plays a clear role, but here, as soon as the first big rain event occurs, the soil moisture arrives near the saturation and the information about an initial spatial heterogeneity is lost. After that first big rain, the evolution continues as if the profile was homogeneous, like in Figure 3.1.

Another way to add heterogeneity is, for example, to consider a variable hydraulic conductivity, namely a non-constant K_s , such as

$$K_s(x) = \begin{cases} \frac{K_{s,loam}}{10} & \text{if } 50 \text{ cm} < x \le 150 \text{ cm} \\ K_{s,loam} & \text{otherwise} \end{cases}$$
 (3.17)

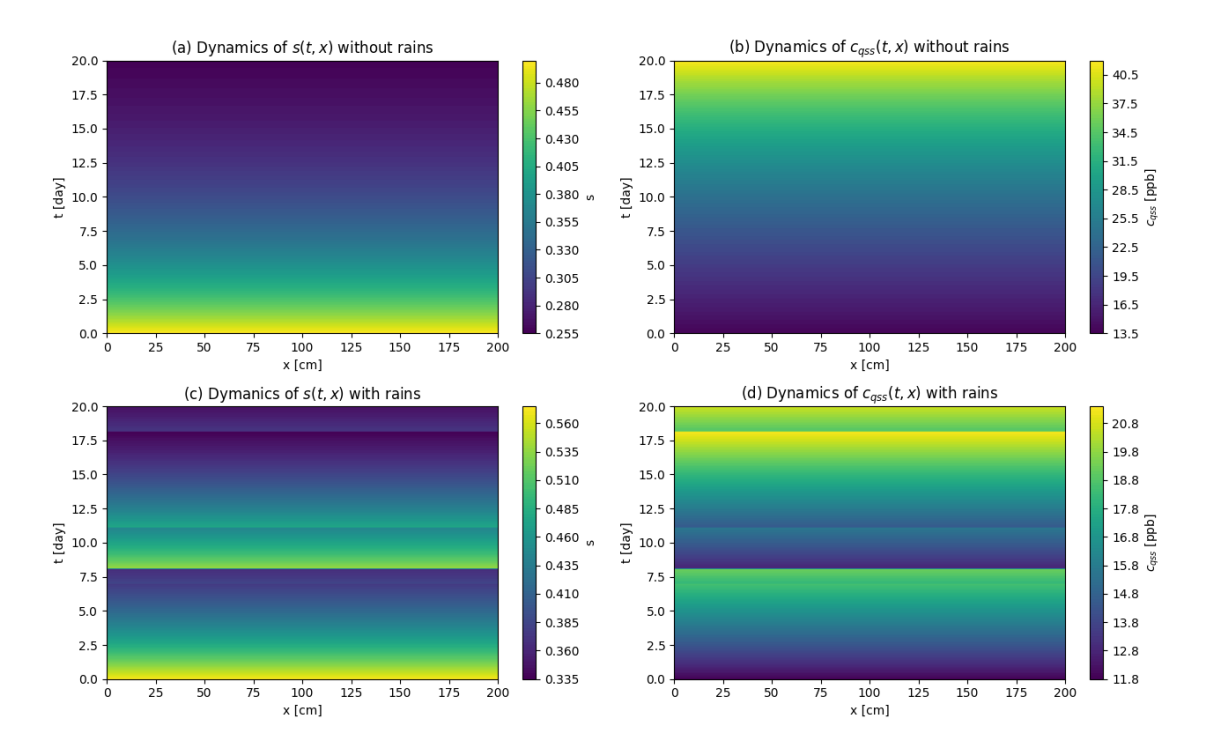


Figure 3.1. Profiles of s(t,x) and c(t,x) for a soil of type loam. In (a) and (b) deterministic simulations have been made, while in (c) and (d) we have considered also the stochastic rain events. The profile is spatially homogeneous since no heterogeneity has been inserted. The parameters of the simulations are: $\lambda = 0.27 \ d^{-1}$, $\alpha = 1.3 \ cm$, $Z = 30 \ cm$, $\delta = 1 \ cm$, $T = 20^{\circ}C$, periodic BCs.

The result of this choice is reported in Figure 3.3. In contrast to what happens in Figure 3.2 just analysed, here the deterministic simulations are exactly as in the homogeneous case since the leakage term, which contains the information about K_s , is important only for high values of soil moisture and hence the different values of K_s do not cause any evident gradients in the profiles. Instead, in the simulations involving also rain events, the leakage term is turned on each time a big rain occurs and the spatial heterogeneity appears.

We could further explore the behaviour of s(t,x) and c(t,x) by considering other functional forms of $K_s(x)$. For example, we can extract its values from a uniform distribution to get more peculiar spatial profiles, as in Figure 3.4 where, again, the determinist case is like the homogeneous one of Figure 3.1, while a wider spectrum of heterogeneity appears at each big rain event in simulations including also stochastic events.

3.3.3 Cases with a non linear D_s

We can now try to make our model a bit more realistic by considering a diffusion coefficient for the soil moisture that is no longer constant. In fact, intuitively, for a realistic case a dependence on the soil moisture itself is expected, similarly to the behaviour of D_c . However, in contrast to it, we imagine that the diffusion coefficient relative to the soil

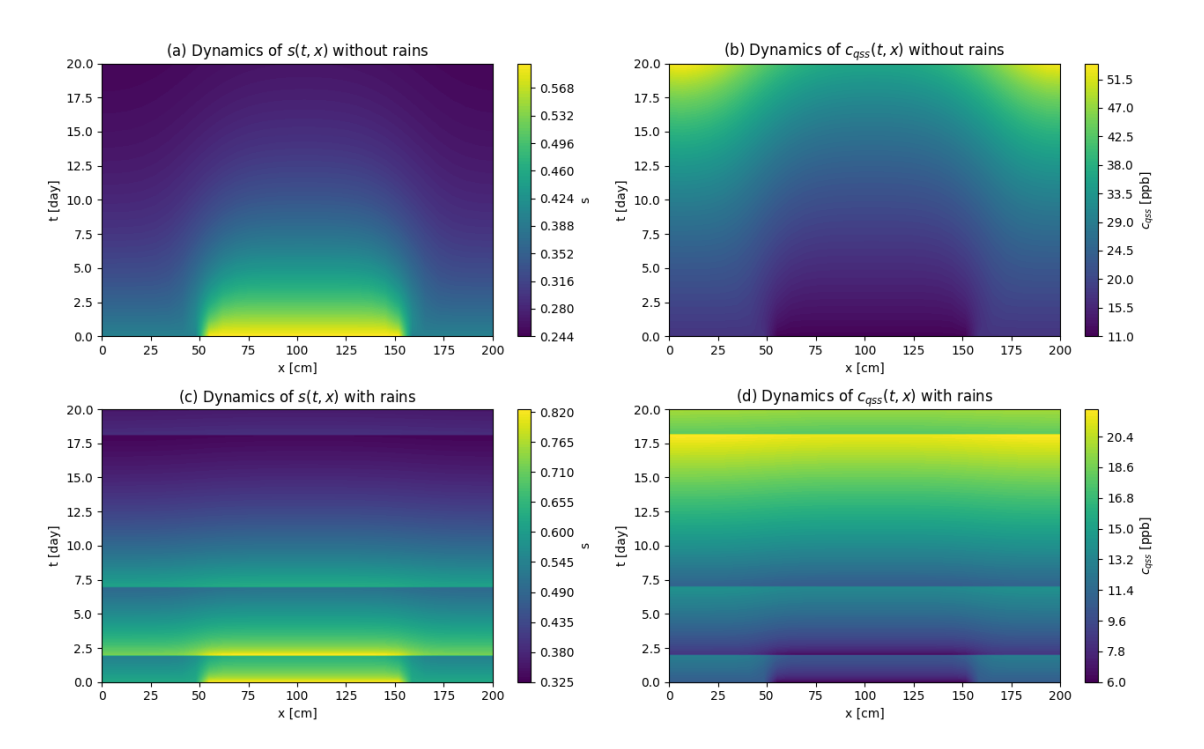


Figure 3.2. Time and spatial evolution of s(t,x) and c(t,x) for a loam soil, considering a constant diffusion coefficient for the soil moisture. In the first row, the two simulations have been made disregarding rain events, while in the second row we have taken into account also stochastic events. Here, the heterogeneity is inserted in the initial condition of s and it is equal to (3.16). The effects of the diffusion, caused by this spatial heterogeneity, are visible, especially in (a) and (b). The parameters of the simulations are: $\lambda = 0.27 \ d^{-1}$, $\alpha = 1.3 \ cm, \ Z = 30 \ cm, \ \delta = 1 \ cm, \ T = 20^{\circ}C$, periodic BCs.

moisture must increase if s(t, x) increases. Therefore, following the advices of "Physical Hydrology" by S. Lawrence Dingman [3] (chapter 8), we choose a relation of this type:

$$D_s(s) = b \cdot |\Psi_{ae}| \cdot K_s \cdot s^{b+2} \tag{3.18}$$

where b is the Campbell parameter, K_c is the saturated hydraulic conductivity and Ψ_{ae} is the air-entry pressure head. This choice is also suggested in order to better link the diffusion coefficient with the hydraulic conductivity that we recall to be a power law in s too, as previously discussed in Eq. (2.19).

Hence, the equation describing the dynamics of s(t, x) that we are going to use in this paragraph is

$$\frac{\partial s(t,x)}{\partial t} = \sum_{i} [y_i \delta(t-t_i)] - \rho(s) + D'_s \left(\frac{\partial s(t,x)}{\partial x}\right)^2 + D_s \frac{\partial^2 s(t,x)}{\partial x^2}$$
(3.19)

where D'_s is the derivative of $D_s(s)$ with respect to s, namely

$$D'_{s}(s) = \frac{dD_{s}}{ds} = b \cdot (b+2) \cdot |\Psi_{ae}| \cdot K_{s} \cdot s^{b+1}$$
(3.20)

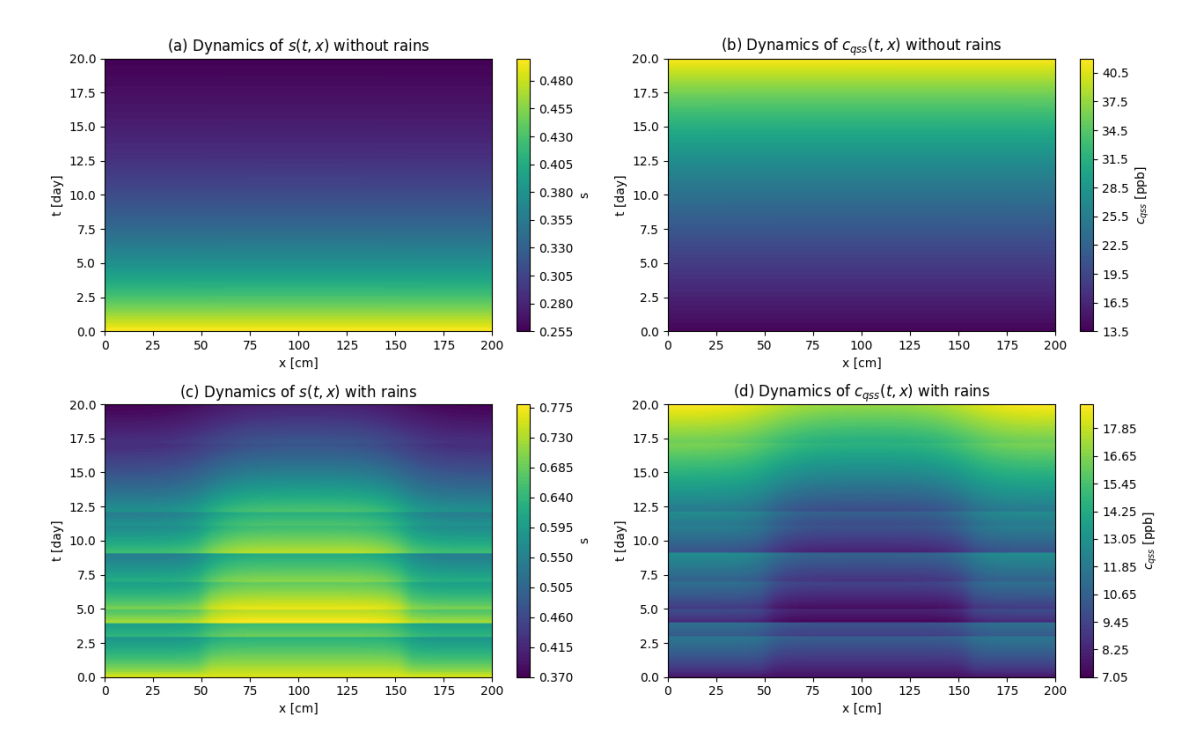


Figure 3.3. Simulations for s(t,x) and c(t,x) in case of a loam soil and a constant diffusion coefficient D_s . Rain events has been disregarded in simulation (a) and (b), while they play an important role in simulations (c) and (d). The spatial heterogeneity has been inserted in the hydraulic conductivity by imposing a profile of the type (3.17); its effects is to generate spatial gradients which activate diffusion, in particular in the stochastic plots. The parameters of the simulations are: $\lambda = 0.27 \ d^{-1}$, $\alpha = 1.3 \ cm$, $Z = 30 \ cm$, $\delta = 1 \ cm$, $T = 20^{\circ}C$, periodic BCs.

Instead, the equation describing the evolution of c(t,x) that we are going to use is eq. (3.13) in the quasi-steady state approximation, exactly as in the previous section.

	b	n	K_s [cm/d]	$ \Psi_{ae} $ [cm]
Sand	4.05	0.395	1520.6	12.1
Loamy sand	4.38	0.410	1347.8	9
Sandy loam	4.90	0.435	299.8	21.8
Loam	5.39	0.451	60.05	47.8
Clay	11.4	0.482	11.06	40.5

Table 3.1. The reported values have been taken from "Physical Hydrology (Chapter 7)" [3].

We are now ready to proceed with the simulations. The same cases as for the constant D_s paragraph have been analysed. Firstly, we report in Figure 3.5 the plot in which the

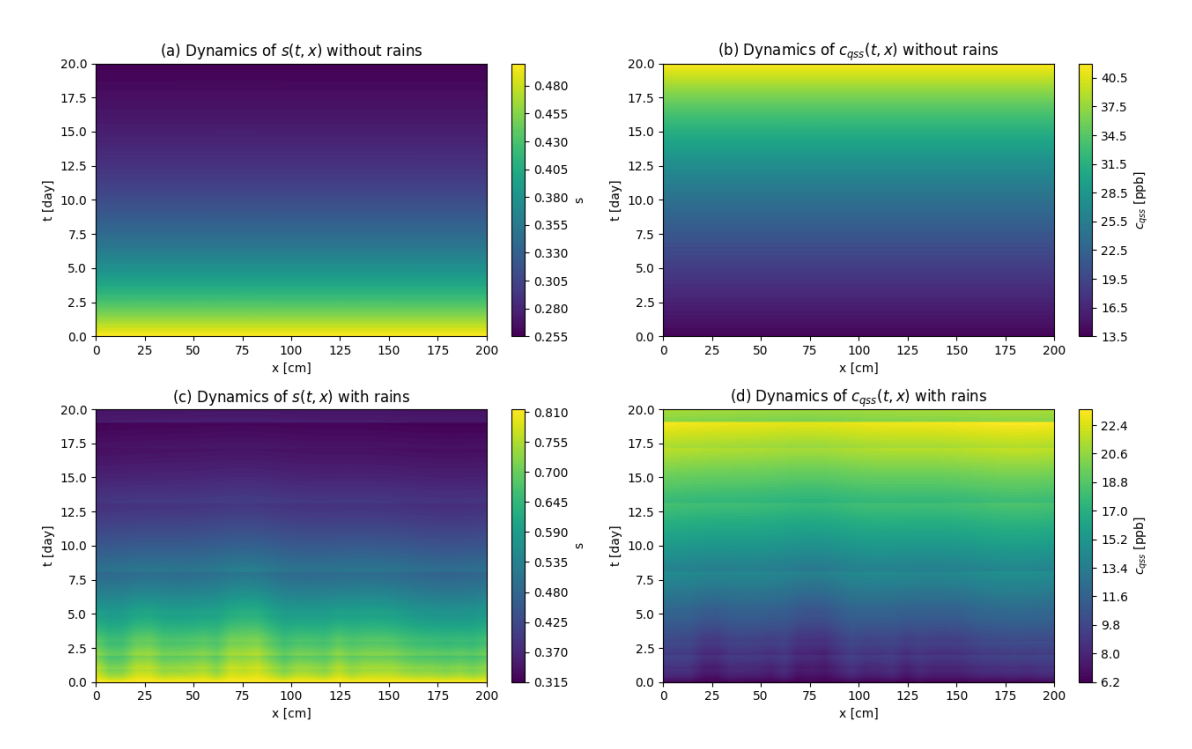


Figure 3.4. Dynamics of s(t,x) and c(t,x) for a loam soil and considering a constant diffusion coefficient D_s . The parameters of the simulations are: $\lambda = 0.27 \ d^{-1}$, $\alpha = 1.3 \ cm$, $Z = 30 \ cm$, $\delta = 1 \ cm$, $T = 20^{\circ} C$, periodic BCs. In (a) and (b) rains have not been considered, whereas in (c) and (d) they have been included. The spatial heterogeneity ha been put in the values of the hydraulic conductivity, which have been extracted from a uniform distribution between 0 and 1. Effects of heterogeneity and hence of diffusion are visible in particular in the stochastic simulation (c) and (d) and generate peculiar spacial profiles.

heterogeneity is inserted in the initial condition of s(t, x); then the two cases with a non-homogeneous K_s are shown in Figure 3.6 and 3.7. In all these graphs, the effects of a non-linear D_s are to accelerate the dampening of the spatial gradients, especially for high values of s. In fact, when the soil moisture gets close to saturation, the diffusion coefficient becomes really big and the diffusion term is dominant.

For longer simulation times, that is, simulations that last years instead of weeks, we can also investigate the time averages of the quantities under study. In Figures 3.8, 3.9 and 3.10 the averages and standard deviations of s(t,x), c(t,x) and $v_d(t,x)$ are reported for the simulations that we have just discussed, respectively, in Figures 3.5, 3.6 and 3.7. They are not the same simulations, since a longer time (about $t_{tot} = 700 \ d$) has been considered, but they have exactly the same parameters. Moreover, only the averages of the stochastic simulations, namely with the rain events, have been computed and here reported. In this study, we also included the quantity $v_d(t,x)$, that is, the deposition velocity. We recall that its definition is

$$v_d(t,x) = \frac{F(s,c)}{c_a}$$

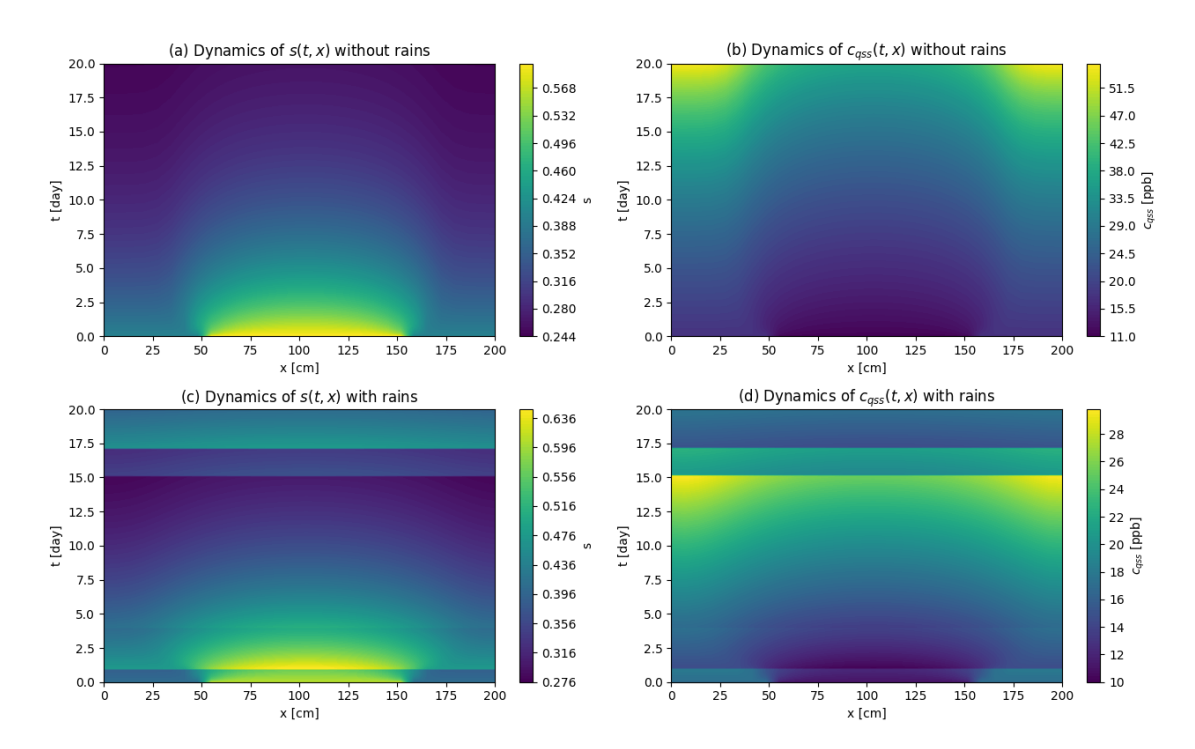


Figure 3.5. Analogous simulations of Figure 3.2, but with a diffusion coefficient D_s which is non linear and given by (3.18). One can see how the diffusion is stronger since it now depends on the values of s. The type of soil is loam and the parameters of the simulations are again $\lambda = 0.27 \ d^{-1}$, $\alpha = 1.3 \ cm$, $Z = 30 \ cm$, $\delta = 1 \ cm$, $T = 20 \ ^{\circ}C$, periodic BCs.

where F is the hydrogen flux from the atmosphere, while c_a is the atmospheric hydrogen concentration. With the addition of diffusion processes, its analytical form cannot be anymore (2.29), but the deposition velocity still remains a crucial quantity that sums up all the limitations involved in the hydrogen uptake, as we discussed at the end of the previous chapter.

In these plots, we can see how the diffusion contribution is important. In fact, the average profiles in all three cases are practically homogeneous, regardless of the heterogeneity inserted. Only a very light slope is present. As an observation, we also put dashed lines in these figures to represent various quantities: $\langle \overline{s} \rangle$, $\langle \overline{c} \rangle$ and $\langle \overline{v}_d \rangle$ are the spatial averages of the time averages (namely the mean values of the blue curves in these plot); whereas $c(\langle \overline{s} \rangle)$ and $v_d(\langle \overline{s} \rangle)$ are, respectively, the hydrogen concentration and the deposition velocity evaluated at the average value of s. In the next section, we will further analyse this point and discuss about why they do not coincide.

3.3.4 α - λ Diagrams

The time and spatial profiles of situations similar to the ones we discussed in the previous two sections are usually used to compute averages. In fact, for the presence of stochastic events such as rains, useful pieces of information are hidden in the mean values

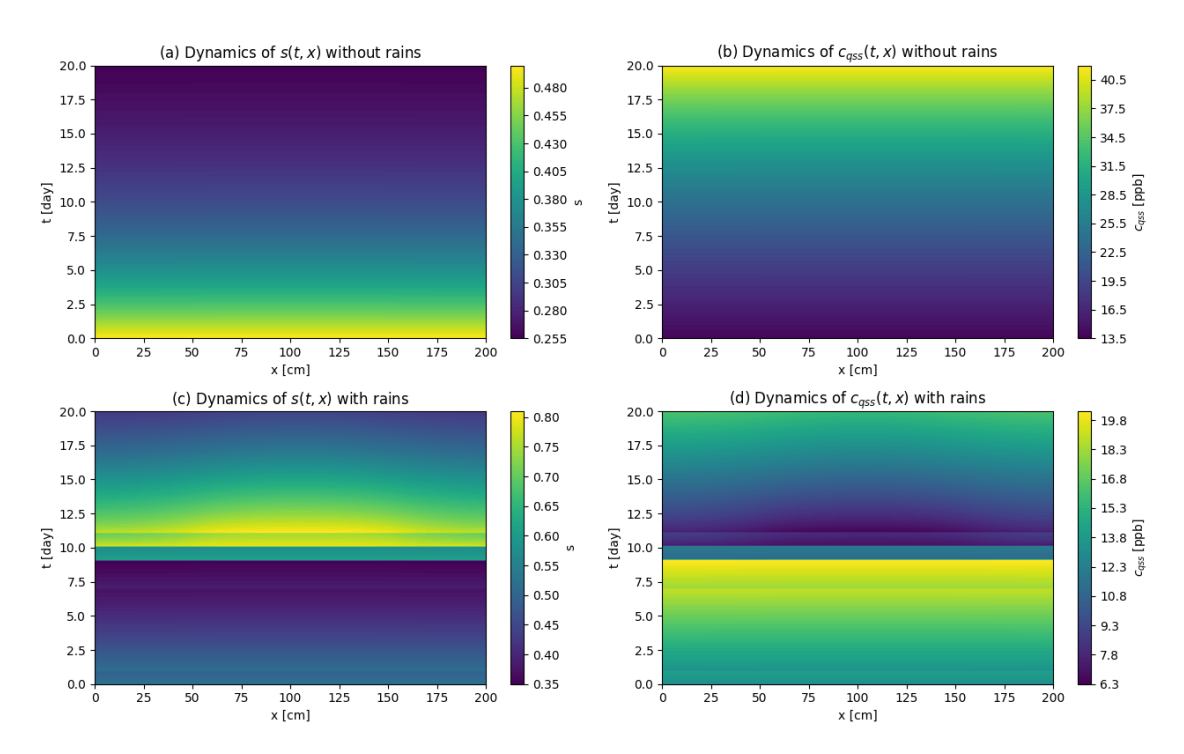


Figure 3.6. Time and space evolution of s(t,x) and c(t,x) for a loam soil. This is the same case as in Figure 3.3, so with heterogeneity inserted in K_s according to (3.17), however we now consider a non linear diffusion coefficient for the soil moisture given by (3.18). While in (a) and (b) spatial gradients are not generated, in (c) and (d) one can see the effect of diffusion and, in particular, we notice how strong it is when s gets bigger then about 0.7. The parameters of the simulations are again: $\lambda = 0.27 \ d^{-1}$, $\alpha = 1.3 \ cm$, $Z = 30 \ cm$, $\delta = 1 \ cm$, $T = 20 \ ^{\circ}C$, periodic BCs.

and standard deviations of the main variables' distributions. In this particular context, however, an erroneous procedure is, sometimes, carried out: to compute the spatial and time averages of quantities such as c(t,x) and $v_d(t,x)$, first the average value of s(t,x) is computed and then c and v_d are evaluated at it, namely for $s = \langle \overline{s} \rangle$. In short, instead of directly computing the time and spatial averages of c and v_d from the profiles obtained from a complete simulation, the approximations $\langle \overline{c} \rangle = c(\langle \overline{s} \rangle)$ and $\langle \overline{v}_d \rangle = v_d(\langle \overline{s} \rangle)$ are made. As we said, these equalities are not true: for the presence of non-linearities in the equations, the average values cannot enter some of the mathematical functions involved in the calculation of c and v_d and $\langle \overline{c} \rangle$ and $\langle \overline{v}_d \rangle$ are actually different from $c(\langle \overline{s} \rangle)$ and $v_d(\langle \overline{s} \rangle)$, as anticipated in Figures 3.8, 3.9 and 3.10 where we plot, in dashed black lines, these four quantities in order to show that they do not coincide.

Still, the approximation discussed above, although generally false, might be valid in some particular cases and its implementation can save a lot of time by avoiding the need of simulations for the c profiles. To better understand this point, we performed a series of simulations keeping all the parameters constant, with the exception of the rates α and λ of the rain events that we allow to vary between (0.1; 0.5) d⁻¹ for λ and (0.25; 2.5) cm

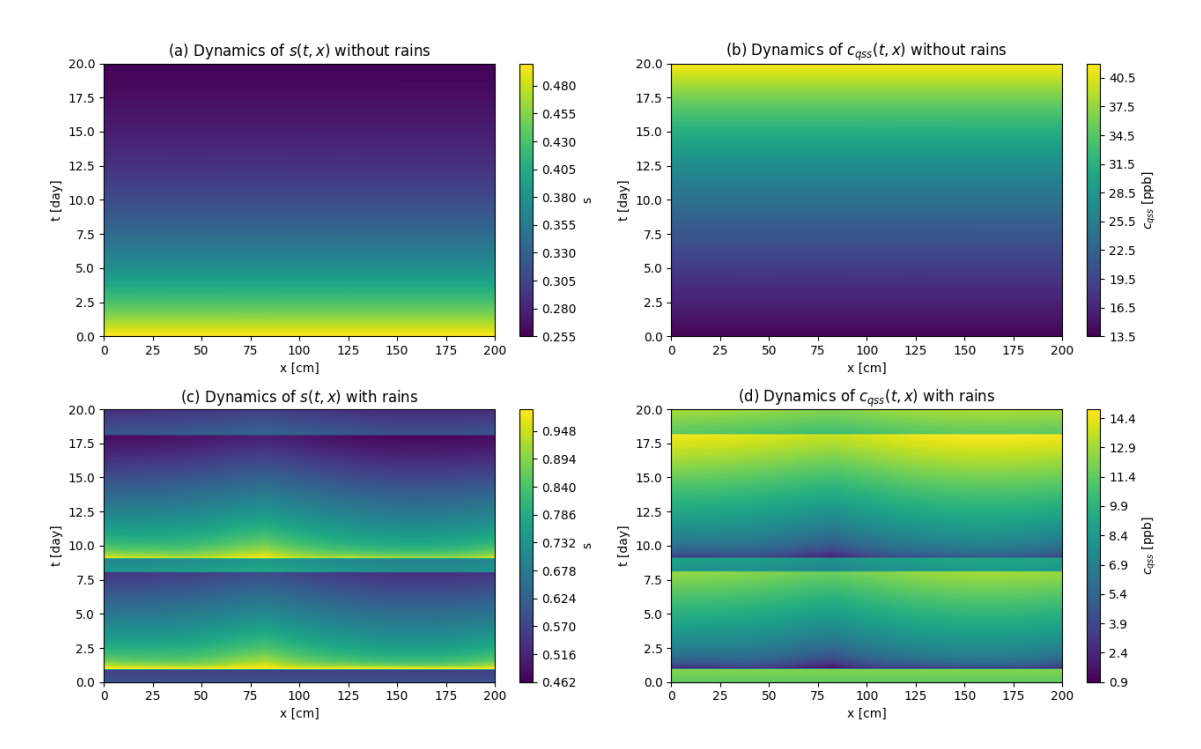


Figure 3.7. Profiles of s(t,x) and c(t,x) for a loam soil and considering a non linear D_s , in contrast to Figure 3.4. The heterogeneity has been inserted in K_s by extracting its values from a uniform distribution. We can see its effects around $t \approx 1$ d and $t \approx 9$ d in (c) and (d) where an heterogeneous spatial profile is quite visible, but quickly smoothed by diffusion that is really strong since s is near saturation. The parameters of the simulations are again: $\lambda = 0.27$ d^{-1} , $\alpha = 1.3$ cm, Z = 30 cm, $\delta = 1$ cm, T = 20 °C, periodic BCs.

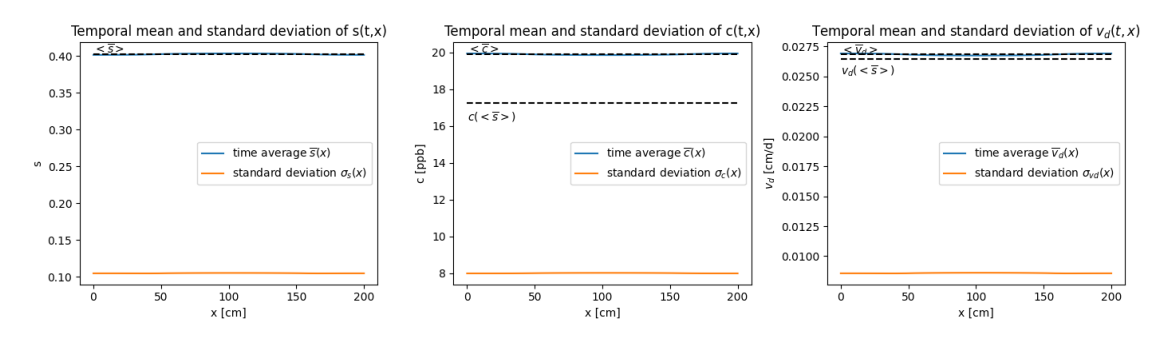


Figure 3.8. Temporal averages and standard deviation of s(t, x) (on the left), c(t, x) (in the middle) and $v_d(t, x)$ (on the right). The simulation parameters are the same as in Figure 3.5, that is, with the heterogeneity put in the initial condition of the soil moisture according with (3.16). The only difference is a longer simulation time of about 700 d.

for α . Moreover, a modification with respect to the simulations of the previous sections has been made: the spatial heterogeneity is no longer inserted artificially into some of the parameters, but a heterogeneous spatial domain has been chosen. In order to have more

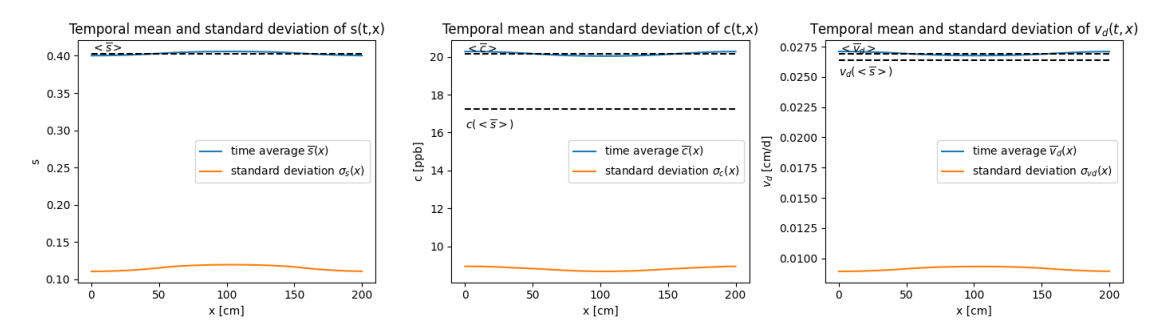


Figure 3.9. Temporal averages and standard deviation of s(t,x) (on the left), c(t,x) (in the middle) and $v_d(t,x)$ (on the right). The simulation parameters are the same as in Figure 3.6, namely with heterogeneity inserted in the hydraulic conductivity as in (3.17). The only difference is a longer simulation time of about 700 d.

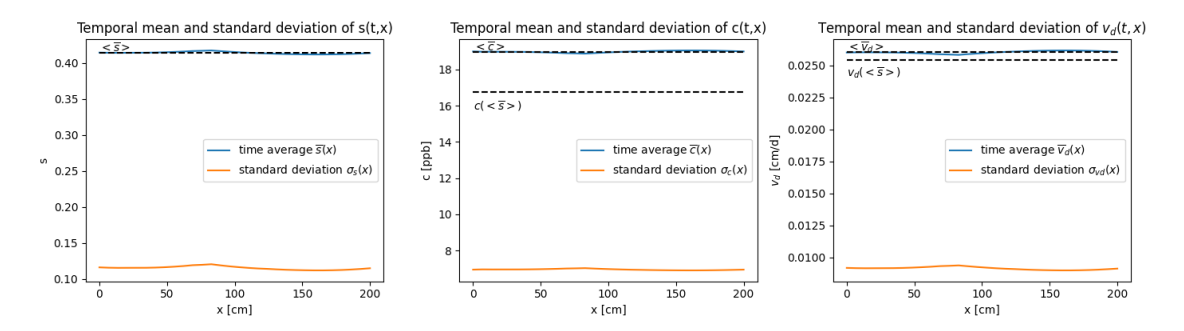


Figure 3.10. Temporal averages and standard deviation of s(t,x) (on the left), c(t,x) (in the middle) and $v_d(t,x)$ (on the right). The simulation parameters are the same as in Figure 3.7, with the heterogeneity put in K_s which has been extracted from a uniform distribution. The only difference is a longer simulation time of about 700 d.

realistic situations, in fact, we now divide our spatial domain into two different soils: half is of a loam type, while the other half is of a sand type. The different properties and features of these two soils translate into different levels of soil moisture and hydrogen, which, in turn, activate the diffusive terms.

The purpose of these simulations was to compute, as functions of the rates α and λ , the ratios:

$$\frac{\langle \overline{c} \rangle}{c(\langle \overline{s} \rangle)} \quad ; \quad \frac{\langle \overline{v}_d \rangle}{v_d(\langle \overline{s} \rangle)} \tag{3.21}$$

and the results are displayed in Figure 3.11, with the iso-p curves representing some of the main climates (p is the precipitation parameter and is equal to $p = \lambda \cdot \alpha$). We can see that the ratios tend to 1 as the precipitation rates grow. This behaviour was somehow expected: the non-linearities encoded in the equations are, in fact, smoothed down by the diffusion terms, which become dominant for high values of soil moisture. Hence, it is possible to approximate $\langle \overline{c} \rangle \approx c(\langle \overline{s} \rangle)$ and $\langle \overline{v}_d \rangle \approx v_d(\langle \overline{s} \rangle)$ for wet climates, thanks to the presence of diffusion processes. Instead, for temperate cold and, in particular, for semi-arid ecosystems, this approximation does not work. In light of what was said in

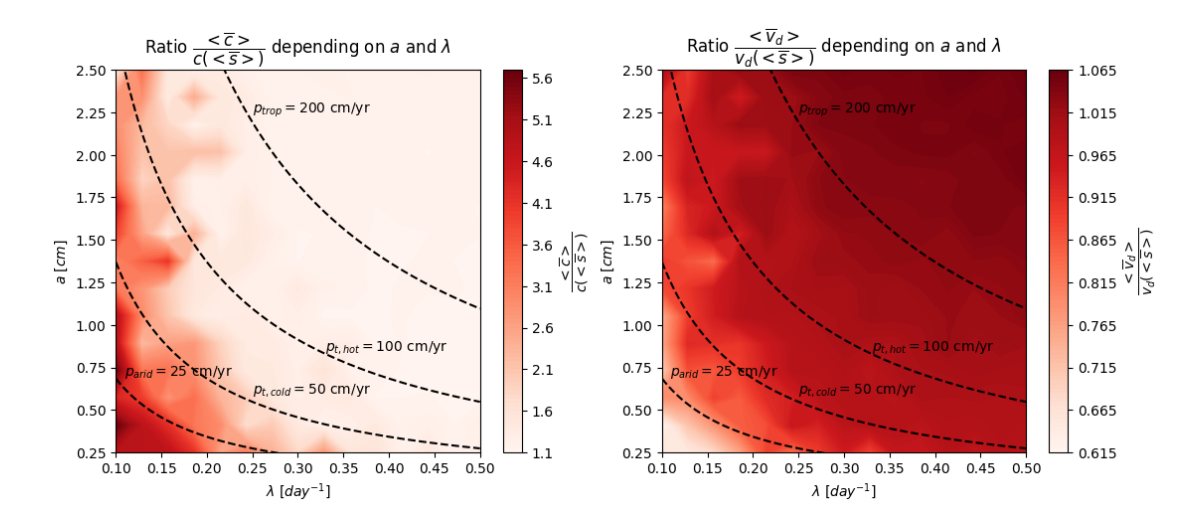


Figure 3.11. The two important ratios are shown in the figures above: on the left one can find $\frac{\langle \overline{c} \rangle}{c\langle (\overline{s}) \rangle}$ while on the right $\frac{\langle \overline{v}_d \rangle}{v_d\langle (\overline{s}) \rangle}$ is reported. Some iso-p curves of the main climates (arid, temperate cold and hot, tropical) are also reported, in order to better highlight in which regimes the approximation is good (the very wet climate for which the ratios are nearly 1) and in which the error is too high (the semi-arid ecosystems). The simulations performed are about 225 and the only parameters which are not constant are λ and α . The others are: a spatial domain of 2 m divided half in sand soil and half in loam soil, $Z_r = 30$ cm, $\delta = 1$ cm, T = 20 °C, $\Delta t = 10^{-5}$ d, $\Delta x \approx 7$ cm, an initial condition for s equal to $s_0 = 0.5$.

Chapter 2, this latter regime is also the most interesting for our study since it is the one which maximizes the hydrogen uptake. Its investigation is, therefore, crucial and must be carried out with great attention.

A similar analysis can be performed for the atmospheric flux contribution. Again, we constructed some $\alpha - \lambda$ diagrams by repeating many simulations in which the only varying parameters are the rates of the rain events α and λ . Furthermore, in this case too the spatial domain is divided half into sand and half into loam, in order to generate the spatial heterogeneity more realistically. This time, however, our aim is to compute the time and spatial average of the vertical flux F(s,c) of H_2 and compare its behaviour when diffusion processes are considered with the one in which the averages are calculated without the diffusion terms. That is, we would like to understand whether the horizontal flux of H_2 , namely that generated by diffusion, has some effects on the vertical flux from the atmosphere. It is, in fact, possible that the diffusion processes, moving the hydrogen stocked in soil, may redistribute the available H_2 in a better way for the bacterial community, increasing its activity and, as a consequence, the consumption of hydrogen, making room for other atmospheric H_2 to enter the soil.

Figure 3.12 shows the results of these simulations. In particular, the ratio between $\langle \overline{F} \rangle$ with and without diffusion has been computed in three different situations: in the left plot, we perform the spatial average only over the loam half of the domain; in the right, instead, the spatial average has been computed only over the sand half of the domain;

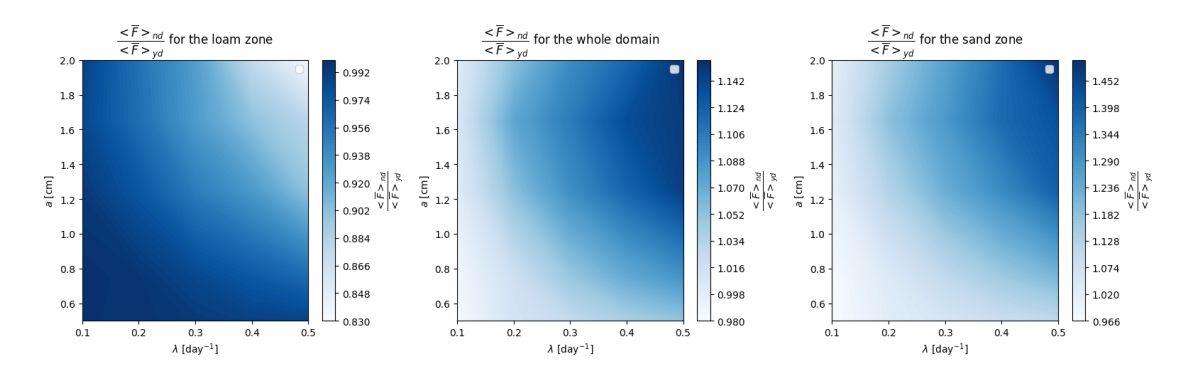


Figure 3.12. In the figure above, the ratio between the average value of the atmospheric flux without diffusion $\langle \overline{F} \rangle_{nd}$ and with diffusion $\langle \overline{F} \rangle_{yd}$ is reported for three different spatial domains: on the left it has been computed only for the loam half of the global domain; on the right the same has been done but only for the sand half of the domain; in the middle, eventually, it is shown the ratio with the average calculated on the whole spatial domain (sand and soil together). In contrast to Figure 3.11, here the ratio tends to 1 for climate with poor precipitations such as semi-arid ecosystems, while differs from it the most for wet climates. The simulations performed are 25 and the main parameters are: a spatial domain of 2 m split into 1 m of sand and 1 m of loam, $Z_r = 30$ cm, $\delta = 1$ cm, T = 20 °C, $\Delta t = 10^{-5}$ d, $\Delta x \approx 7$ cm, $s_0 = 0.5$.

finally, in the middle plot, we make the calculation over the entire spatial domain. One can see that the three plots show similar trends: all of them have the ratio that tends to 1 as the precipitation rates decrease, namely for semi-arid climates, while the main differences between the cases with and without diffusion are observable for high values of α and λ .

These results too were in some sense expected, since, as we have said many times, diffusion processes become more and more important as s tends to 1, and this happens especially when precipitations are high. In contrast, the diffusion terms become small for ecosystems with low values of soil moisture. Thus, it stands to reason that the main differences between $\langle \overline{F} \rangle_{yd}$ and $\langle \overline{F} \rangle_{nd}$ occur for very wet climates, where the diffusion terms are stronger and can indeed make a difference.

Instead, what is not so obvious is that diffusion processes can increase the activity of the bacterial community, but they could also hinder it and this depends on the hydrologic regime we are in. From Figure 3.12 it is, in fact, clear that the ratios are less than 1 for semi-arid conditions, namely $\langle \overline{F} \rangle_{nd} < \langle \overline{F} \rangle_{yd}$, which means that, here, the diffusion terms enhance the atmospheric flux. In contrast, we have $\langle \overline{F} \rangle_{nd} > \langle \overline{F} \rangle_{yd}$ for high values of the precipitation rates, that is, in the wet regime diffusion lowers the atmospheric flux of H_2 .

In order to deeply understand this behaviour, we performed two single simulations, one for a semi-arid climate and the other for a wet ecosystem, in which we computed the time averages of some of the main quantities involved in this discussion. Again, a comparison has been made between the same averages with and without diffusion. In Figures 3.13 and 3.14, these comparisons are reported: in the first, one can find the time averages of s(t,x) and $c_{qss}(t,x)$ for both cases; in the second, we analyse the horizontal and vertical fluxes and the biological decay term.

The effects of diffusion processes are clear in the plots (b) and (d) of Figure 3.13, where the profiles of s and c smoothly join up between the two different regions of soil. However, the most interesting effects are visible at the interfaces between the loam zone and the sand zone in (c). Here, in fact, diffusion is capable of generating complex spatial patterns with sharp minima at the edges of the sand regions and local maxima at those of the loam zone. While the diffusion of the soil moisture in the semi-arid case is quite small, that of c is, instead, considerably high (as displayed in (e) and (g) Figure 3.14), and is sufficient to strongly redistribute the soil hydrogen at the interfaces. This redistribution is also responsible for increasing both the biological decay and the vertical flux of H_2 that, in this case, are higher than their twins in the simulation without the diffusion terms. This behaviour confirms what we have already discussed in Figure 3.12 where we said that $\langle \overline{F} \rangle_{nd} < \langle \overline{F} \rangle_{yd}$ for low values of the precipitation rates.

Concerning the other case, namely the wet climate, we can see how high levels of soil moisture produce a strong diffusion of s but a weak diffusion of hydrogen (Figures (f) and (h) of 3.14), and this is due to the fact that all the pores of the soil are, in this case, filled with water. Thus hydrogen, which is much less on average than in the semi-arid case, cannot easily diffuse in the horizontal direction. The vertical flux and the biological decay term are also hindered by the presence of large quantity of water and are even weakened by the action of the diffusion of s.

Therefore, although the biggest differences between $\langle \overline{F} \rangle_{yd}$ and $\langle \overline{F} \rangle_{nd}$ appear in the wet regime, they are due to the presence of strong diffusion processes of soil moisture that actually diminish the hydrogen uptake. In contrast, in the semi-arid regime, the vertical flux of H_2 is enhanced by low soil moisture levels and by the horizontal diffusion of the hydrogen concentration, especially at the interfaces between different soil types where a sequence of global minima and local maxima arises. Further studies with different types of heterogeneity may be needed to better investigate this latter phenomenon, but, in the context of H_2 uptake, the different behaviour of these two opposite regimes is highlighted in both $\alpha - \lambda$ diagrams we discussed.

3.3.5 Check on the validity of the quasi-steady state approximation in 1D

To conclude the discussion about the 1D model, we return to a topic that we have put on hold: the comparison between the complete solution of Eq. (3.13) and its quasi-steady state approximation, which, as we said, we have used throughout the whole chapter.

We tried a simulation similar to those made in the paragraph about the D_s constant cases, but with fewer simulation days. In fact, we already mentioned that with the complete equation the simulation time could become really long and so only short simulation can be achieved in a runnable time. For what concerns the parameters, we go back to the situations in which the soil is of a uniform type (in this case we chose a loam one) in which the heterogeneity has been inserted through the initial condition of s(t, x), as in Figure 3.2. In particular, we define an initial value that is equal to:

$$s_0(x) = \begin{cases} 0.6 & \text{if } 25 \text{ cm} < x \le 75 \text{ cm} \\ 0.4 & \text{otherwise} \end{cases}$$
 (3.22)

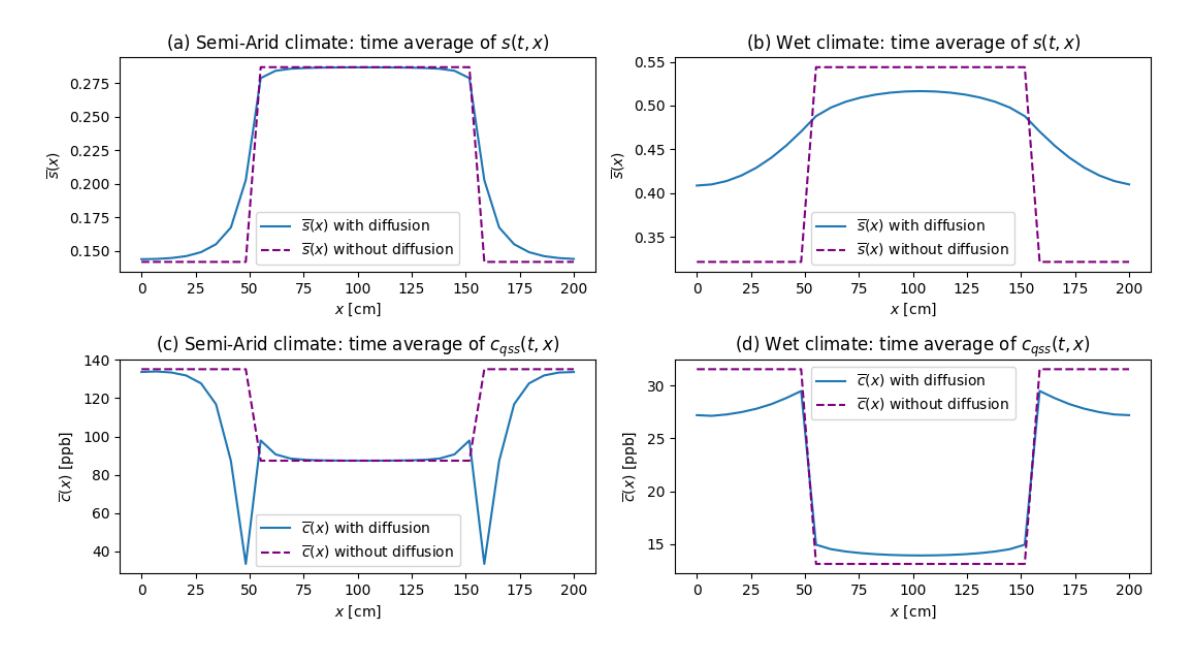


Figure 3.13. Time average of s(t,x) (first raw) and $c_{qss}(t,x)$ (second raw) for two simulations: on the left column a semi-arid climate has been analysed, whereas on the right column the results for a wet case have been reported. In all plots, the comparison between the simulations with (in blue) and without (in purple) the diffusion terms is visible. As expected, for the wet case the diffusion makes the profiles much more different than for the semi-arid case, although complex patterns arise at the interfaces between the two soils in c_{qss} for the semi-arid climate. The rates of rain events chosen are $(\lambda,\alpha)=(0.14~{\rm d}^{-1},0.5~{\rm cm})$ for the semi-arid simulation and $(\lambda,\alpha)=(0.45~{\rm d}^{-1},1.9~{\rm cm})$ for the wet case. The other main parameters, kept constant in the simulations, are: a spatial domain of 2 m divided half into loam (center of the plots) and half into sand (edges of the plots), $Z_r=30~{\rm cm}$, $\delta=1~{\rm cm}$, $T=20~{\rm cm}$, $\Delta t=10^{-5}~{\rm d}$, $\Delta x\approx7~{\rm cm}$, $s_0=0.5$, periodic boundary conditions.

In this framework, we also need an initial condition for c(t,x), strictly required to solve equation (3.13); we then choose to define c_0 as the corresponding quasi-steady state value of s_0 , computed by means of (2.28). Thus, we get that the initial values either of the complete solution and of its quasi-steady state approximation are the same, unless a rain event does take place at t=0. In this case, the two profiles will start with different values but, after few steps, they will converge.

In Figure 3.15 the comparisons we have talked about are reported. In the first row, the case in which the rain events are disregarded has been analysed, while in the second row one can find what happens if we also take the rains into account. We can see that the profiles of $c_{complete}$ and c_{qss} both in (b) and (c) and also in (e) and (f) are equal, confirming the validity of the quasi-steady state approximation also in 1D. Moreover, we tried to investigate in Figure 3.16 a single time series of $c_{complete}$ and c_{qss} by fixing the position at $x \approx 30$ cm, and again the two profiles superimpose quite perfectly, both with and without considering rain events.

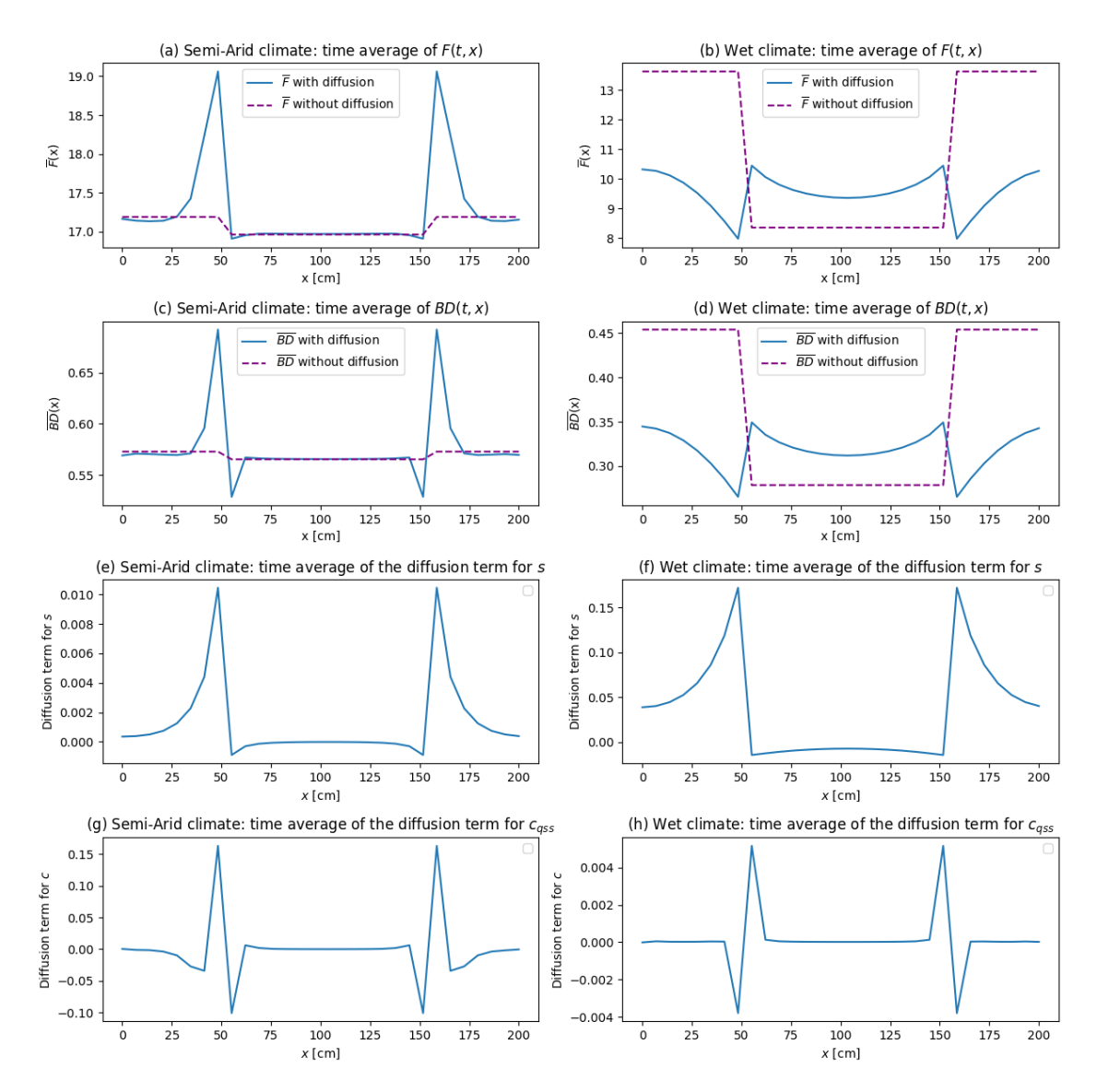


Figure 3.14. In this figure, the time averages of the same quantity have been computed for a semi-arid climate (left column) and a wet ecosystem (right column). In the first row, the average of the vertical flux F(t,x) of hydrogen is reported; in the second, the biological decay term BD(t,x) is shown; finally, in the last two rows, the diffusion terms of soil moisture and hydrogen are displayed. In order to compare the profiles, the same averages of twin simulations without diffusion of both s and c are shown in the first four plots. The rates of rain events chosen are $(\lambda,\alpha)=(0.14~{\rm d}^{-1},0.5~{\rm cm})$ for the semi-arid simulation and $(\lambda,\alpha)=(0.45~{\rm d}^{-1},1.9~{\rm cm})$ for the wet case. The other main parameters, kept constant between the simulations, are: a spatial domain of 2 m divided half into loam (center of the plots) and half into sand (edges of the plots), $Z_r=30~{\rm cm}$, $\delta=1~{\rm cm}$, $T=20~{\rm cm}$, $\Delta t=10^{-5}~{\rm d}$, $\Delta x\approx 7~{\rm cm}$, $s_0=0.5$, periodic boundary conditions.

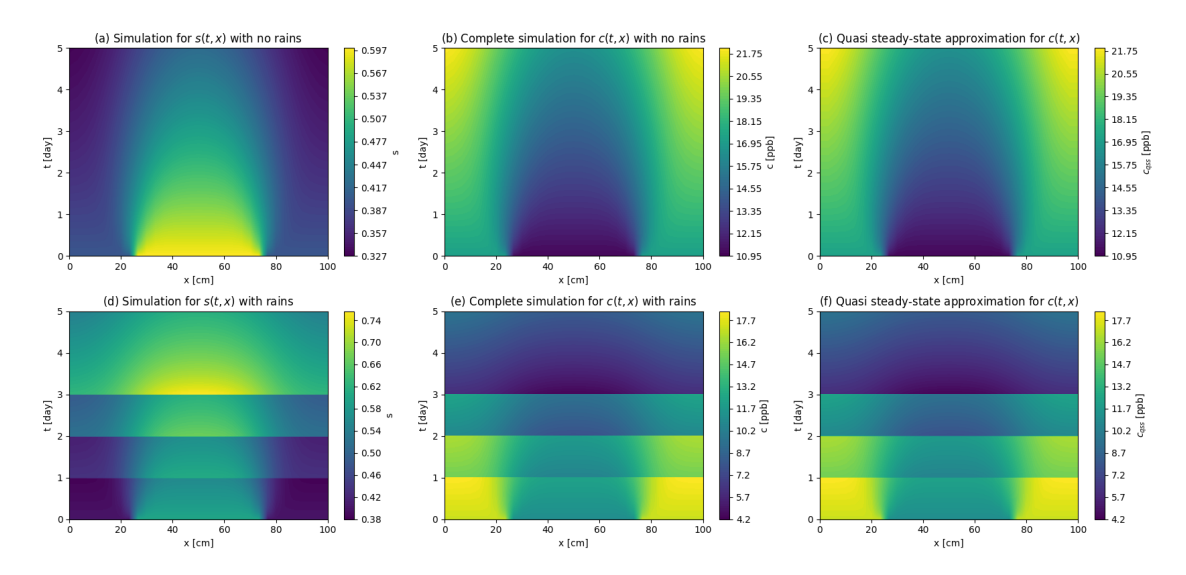


Figure 3.15. Comparison between the solution of the complete equation for c(t,x), namely Eq. (3.13), and its quasi-steady state approximation obtain in Appendix A. Firstly, we report the profile of s(t,x) on the left side (plot (a) and (d)); then we show the solution of the complete equation in (b) and (e); finally, at the right side of the figure, one can find the quasi-steady state approximation for c(t,x). The upper graphs have been obtained without considering the rain events, while the second triplet takes rains into account. The main parameters of the simulations are: soil of type loam, $D_s = \text{const} \approx 18 \text{ cm}^2/\text{day}$, $\lambda = 0.7 \text{ day}^{-1}$, $\alpha = 2.5 \text{ cm}$, Z = 30 cm, $T = 20 \, ^{\circ}C$, $\delta = 1 \text{ cm}$.

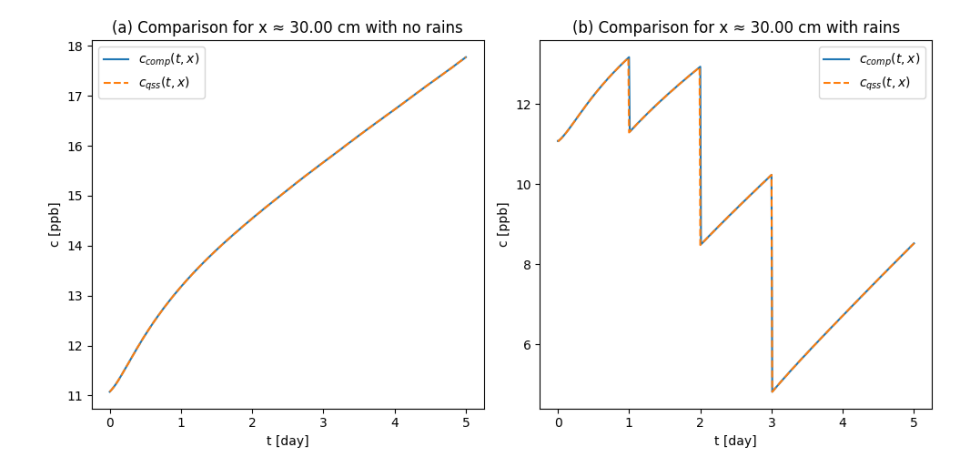


Figure 3.16. Comparison at fixed x between the complete solution for c(t,x) and its quasi-steady state approximation. The time series shown correspond to the profiles in Figure 3.15 taken for $x \approx 30$ cm. In particular, (a) is referred to the plots (b) and (c) of Figure 3.15, while (b) corresponds to the graphs (e) and (f), again of Figure 3.15. The profiles superimpose perfectly, confirming the validity of the quasi-steady state approximation also for the 1D model.

3.4 2D model

We would like to end the chapter and, with it, the whole thesis by investigating, although in an introductory way, what happens if we extend the spatial domain from 1D to 2D.

Now, thus, the equations describing our model have to also take the y direction into account and are slightly different from Eqs. (3.19) and (3.13) used in the 1D case. They are:

$$\begin{cases}
\frac{\partial}{\partial t}s(t,x,y) = \sum_{i}[y_{i}\delta(t-t'_{i})] - \rho(s) + \vec{\nabla} \cdot [D_{s}\vec{\nabla}s(t,x,y)] \\
\frac{\partial}{\partial t}c(t,x,y) = \frac{1}{(1-s)} \left[\frac{F(s,c) - Z_{r} \cdot BD(s,c)}{nZ_{r}} + c\frac{\partial s}{\partial t} \right] + \vec{\nabla} \cdot [D_{c}\vec{\nabla}c(t,x,y)]
\end{cases}$$
(3.23)

which, considering the non-linear form (3.18) for D_s and the relation (2.23) for D_c , turn into

$$\begin{cases}
\frac{\partial s}{\partial t} = \sum_{i} [y_{i}\delta(t - t'_{i})] - \rho(s) + D'_{s}(s)(\vec{\nabla}s)^{2} + D_{s}(s)\nabla^{2}s \\
\frac{\partial c}{\partial t} = \frac{1}{(1 - s)} \left[\frac{F(s, c) - Z_{r} \cdot BD(s, c)}{nZ_{r}} + c\frac{\partial s}{\partial t} \right] + D'_{c}(\vec{\nabla}s) \cdot (\vec{\nabla}c) + D_{c}\nabla^{2}c
\end{cases}$$
(3.24)

As in the section dedicated to the 1D model, also here for the dynamics of the hydrogen concentration in soil the quasi-steady state approximation is performed in order to reduce the running time otherwise too long for our purposes. The 2D version of this approximation is derived in Appendix A.

Firstly, we try a simulation where the spatial domain chosen is mathematically defined as a chessboard-like pattern of sand and loam zones. Clearly it is not a realistic case, but still it can tell us interesting clues. In particular, we opted for a 400×400 cm spatial domain divided into 16 squares of side equal to 1 m. In Figure 3.17, we show the profiles of s(t, x, y) and $c_{qss}(t, x, y)$ for a generic time instant equal to t = 350 d, whereas in Figure 3.18 the time averages, again of the soil moisture and H₂ concentration, are reported. In particular, in the first two plots of Figure 3.18, we displayed the averages as functions of both the horizontal directions, while, in the second pair of plots, the y has been arbitrarily fixed at 200 cm and the averages are free to vary only in the x direction. These latter graphs, in particular, show great analogies with their twins in one dimension (such as Figure 3.13), where maxima in the loam regions alternate with minima in the sand zones for the soil moisture, while the opposite behaviour occurs for c. Furthermore, in the plot of c, also in the 2D case local maxima and minima appear at the interfaces between sand and loam, although they are much less important with respect to what happens in Figure 3.13 since the hydrologic regime we are in is now different. In fact, in this section, we put ourselves in a temperate climate to avoid the extreme cases of very wet and arid ecosystems previously treated.

Then, we have tried a more realistic scenario where the 2D spatial domain is no longer so mathematically defined as before. Again, we used two different soil types, sand and loam, but we built an interpolation surface to link different points randomly picked and associated with values that vary from sand to loam. In this way, the resulting texture shows a central region of soil very close to a sand type surrounded by a ring-shaped zone

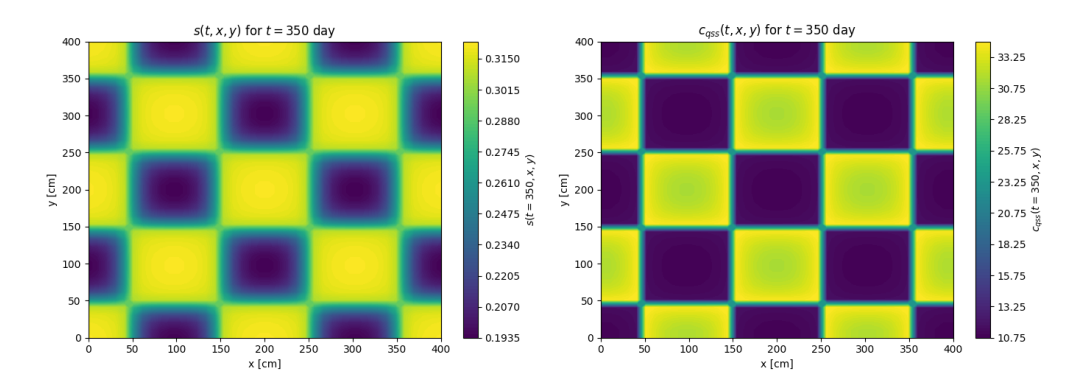


Figure 3.17. The figure shows the spatial profiles of s(t,x,y) (on the left) and $c_{qss}(t,x,y)$ (on the right) for a fixed time instant arbitrarily chosen to be t=350 d, namely at half of the simulation. A chessboard-like 2D domain has been used, where sand zones (darker in the s plot) alternate with loam zones, giving rise to a peculiar spatial pattern. The parameters employed in the simulation are: $\Delta t = 10^{-5}$; $\Delta x \approx 10.26$ cm; $\lambda = 0.2$ d⁻¹ and $\alpha = 1.0$ cm; $\delta = 1$ cm; T = 20 °C; $s_0 = 0.5$; periodic boundary conditions.

that gradually turns into loam. In Figure 3.19, the profiles of s(t,x,y) and c(t,x,y) are reported in the new spatial domain, again for a fixed time instant t=350 day. The wider spectrum of heterogeneity activates the diffusion processes of both moisture and hydrogen, which show odd spatial patterns. In Figure 3.20, the time averages of s(t,x,y) and c(t,x,y) have been computed and reported. As in Figure 3.18, the first pair of graphs show the averages as functions of both x and y, while, in the second, they are displayed at fixed y. Again, in these latter plots, thanks to the choice of the y value that is 250 cm, one can clearly see the sequence of high soil moisture in the semi-loam regions and low s values in the sand-like center zone of the domain. This behaviour is reproduced upside down for the hydrogen concentration in soil, as expected. Also in this case, local maxima and minima are present at the interfaces between different soil types, generated, as we discussed in previous sections, by diffusion processes.

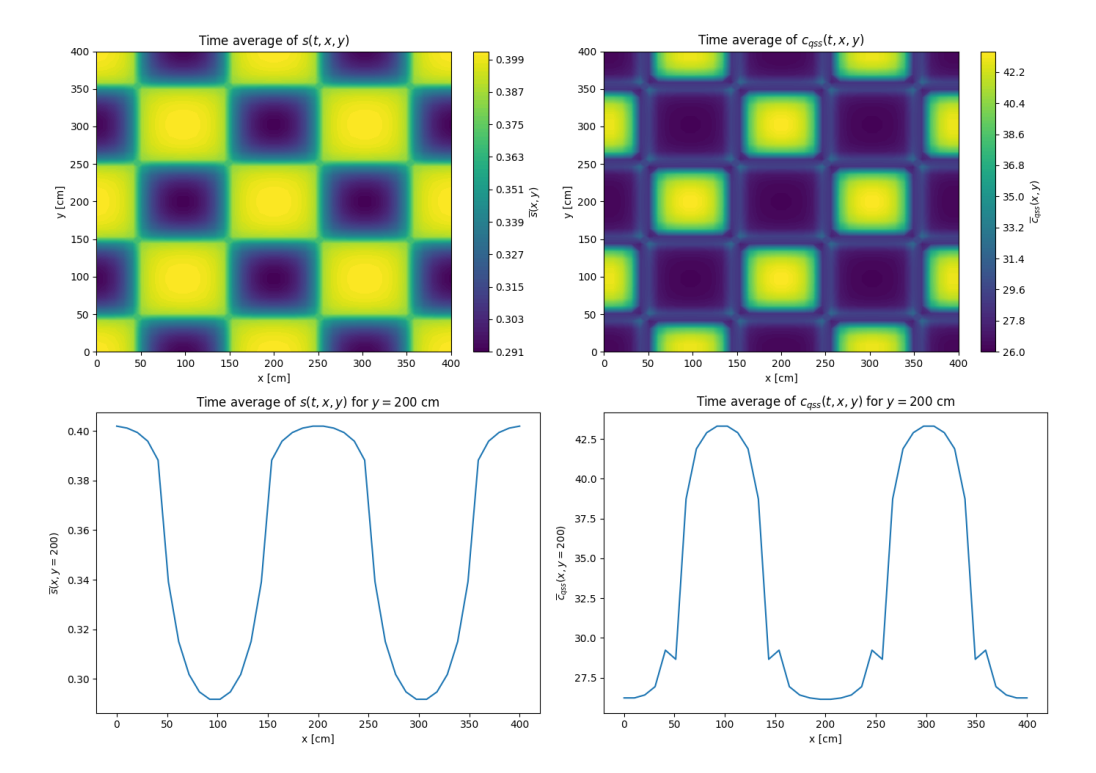


Figure 3.18. Time averages of s(t,x,y) (left column) and $c_{qss}(t,x,y)$ (right column) are reported in the figure above. In particular, in the first row, it is possible to find the spatial profiles of the averages as a function of both x and y, whereas, in the second row, the averages are reported at fixed y, chosen equal to y=200 cm, and one can see an alternation of maxima and minima depending on whether we are in the loam or in the sand zone. The parameters of the simulation are: $\Delta t = 10^{-5}$; $\Delta x \approx 10.26$ cm; $\lambda = 0.2$ d⁻¹ and $\alpha = 1.0$ cm; $\delta = 1$ cm; T = 20 °C; $s_0 = 0.5$; periodic boundary conditions.

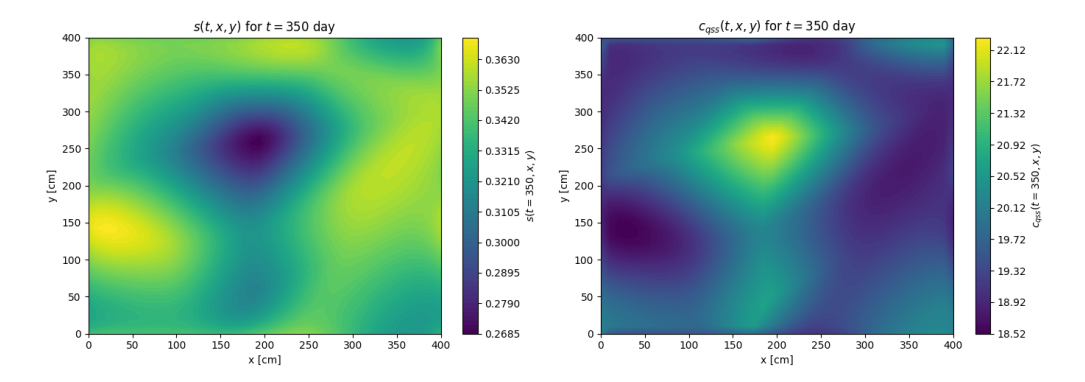


Figure 3.19. A more realistic 2D domain has been chosen for the simulation shown in the figure above, where a surface of interpolation has been used to link zone of type sand with others of type loam. The result is a central region of sand surrounded by a ring-like soil that smoothly turns into loam. On the left plot the spatial profile of s(t,x,y) is reported, while, on the right, one can find that of $c_{qss}(t,x,y)$, both of them at fixed time that we arbitrarily chose to be t=350 day. The parameters of the simulation are: $\Delta t=10^{-5}$; $\Delta x\approx 10.26$ cm; $\lambda=0.2$ d⁻¹ and $\alpha=1.0$ cm; $\delta=1$ cm; T=20 °C; $s_0=0.5$; periodic boundary conditions.

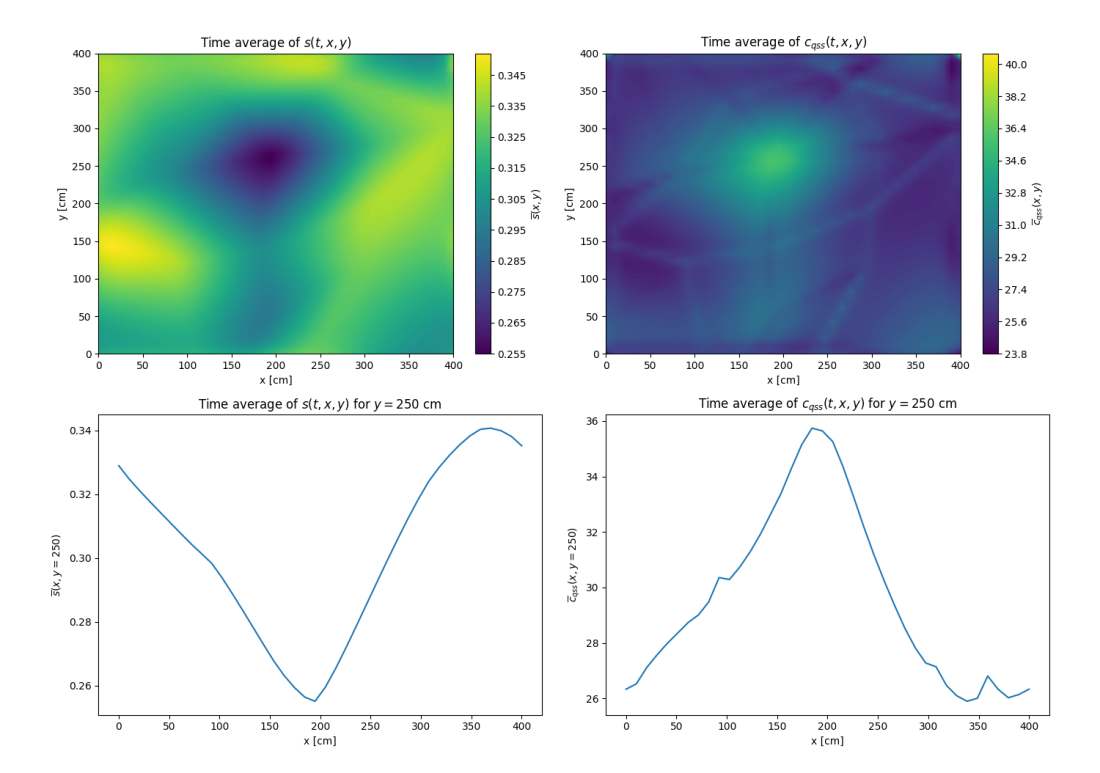


Figure 3.20. Temporal means of s(t,x,y) (left column) and c_{qss} (right column) of the simulation shown in Figure 3.19. Again, in the first row, the spatial profiles are reported as functions of both x and y, while, in the second row, only the dependency on the x variable remains whereas y is fixed to 250 cm. The parameters of the simulation are: $\Delta t = 10^{-5}$; $\Delta x \approx 10.26$ cm; $\lambda = 0.2$ d⁻¹ and $\alpha = 1.0$ cm; $\delta = 1$ cm; T = 20 °C; $s_0 = 0.5$; periodic boundary conditions.

Appendix A

Derivation of the 1D and 2D Quasi-Steady State Approximation

A.1 1D case

As we said in the section about the 1D model, in order to obtain the quasi-steady state approximation we have to solve

$$\frac{\partial^2}{\partial x^2}c + \frac{D_c'}{D_c}\frac{\partial s}{\partial x}\frac{\partial c}{\partial x} = -\frac{1}{nZ_r(1-s)D_c}[F(s,c) - Z_r \cdot BD(s,c)] \tag{A.1}$$

namely a Poisson-like equation. It is, in fact, in the form of a general Poisson equation with variable coefficients such as, in $D \ge 1$,

$$\vec{\nabla} \cdot [u(\vec{r})\nabla\varphi(\vec{r})] = f(\vec{r}) \tag{A.2}$$

where u and f are given scalar functions of the position, that in our case are, respectively, $D_c(s)$ and $\frac{-1}{nZ_r(1-s)}[F(s,c)-Z_r\cdot BD(s,c)]$, while φ is the scalar field we want to find, which for us is c(x).

There are a lot of methods to solve this type of equation; here we chose the Finite-Difference Method, which is one of the simplest. The idea is, as suggested by its name, to substitute the space derivatives with their finite-differences approximation and solve the resulting equation numerically.

So, we start by defining a 1-dimensional spatial grid with N_x discrete points, distanced Δx from each other and labelled by the index $i=0,1,\ldots,N_x-1$. We will also consider periodic boundary conditions, so that the N_x -th position is equal to the i=0 one. Therefore, we can say that the derivatives of s and c, represented momentarily together by a generic function h, can be approximated to

$$\frac{\partial^2 h(x)}{\partial x^2} = \frac{h(x + \Delta x) - 2h(x) + h(x - \Delta x)}{\Delta x^2} \quad ; \quad \frac{\partial h}{\partial x} = \frac{h(x + \Delta x) - h(x)}{\Delta x}$$

and then, using the grid points, we can define

$$h(x) = h_i$$
 ; $h(x \pm \Delta x) = h_{i\pm 1}$

obtaining

$$\frac{\partial^2 h(x)}{\partial x^2} = \frac{h_{i+1} - 2h_i + h_{i-1}}{\Delta x^2} \quad ; \quad \frac{\partial h}{\partial x} = \frac{h_{i+1} - h_i}{\Delta x}$$

After these considerations, we can now see what happens to our equation (??) in the Finite-Difference Method:

$$\frac{\partial^{2}}{\partial x^{2}}c(x) + \frac{D'_{c}}{D_{c}}\frac{\partial s(x)}{\partial x}\frac{\partial c(x)}{\partial x} = \frac{F(s,c) - Z_{r} \cdot BD(s,c)}{nZ_{r}(1-s(x))D_{c}}$$

$$\frac{c_{i+1} - 2c_{i} + c_{i-1}}{\Delta x^{2}} + \left(\frac{D'_{c}}{D_{c}}\right) \cdot \frac{s_{i+1} - s_{i}}{\Delta x} \cdot \frac{c_{i+1} - c_{i}}{\Delta x} = \frac{Z_{r} \cdot BD(s_{i}, c_{i}) - F(s_{i}, c_{i})}{nZ_{r}(1-s_{i})D_{c}}$$

$$c_{i+1} - 2c_{i} + c_{i-1} + \left(\frac{D'_{c}}{D_{c}}\right)(s_{i+1} - s_{i})(c_{i+1} - c_{i}) = \frac{\Delta x^{2} \left[Z_{r}k_{m}h(T)f(s_{i})c_{i} - g_{T}(s_{i})(c_{a} - c_{i})\right]}{nZ_{r}(1-s_{i})D_{c}}$$

for the sake of simplicity, we can group together some of the coefficients of $c_{i\pm 1}$ and c_i defining

$$A(s_i) = \frac{\Delta x^2 Z_r k_m h(T) f(s_i)}{n Z_r (1 - s_i) D_c} \quad ; \quad B(s_i) = \frac{\Delta x^2 g_T(s_i)}{n Z_r (1 - s_i) D_c}$$

so that our equation becomes:

$$c_{i+1} - 2c_i + c_{i-1} + \left(\frac{D'_c}{D_c}\right)(s_{i+1} - s_i)(c_{i+1} - c_i) = A(s_i)c_i - B(s_i)c_a + B(s_i)c_i$$

Although this equation is correct, written like that it is not symmetric in the first-order term, namely the one coming from the first derivatives of s and c. Hence, we can symmetrize it in this way:

$$\left(\frac{D_c'}{D_c}\right) \frac{\partial s}{\partial x} \frac{\partial c}{\partial x} = \left(\frac{D_c'}{D_c}\right) \cdot \frac{1}{2} \left[\frac{s_{i+1} - s_i}{\Delta x} + \frac{s_i - s_{i-1}}{\Delta x}\right] \cdot \frac{1}{2} \left[\frac{c_{i+1} - c_i}{\Delta x} + \frac{c_i - c_{i-1}}{\Delta x}\right] = \\
= \left(\frac{D_c'}{D_c}\right) \cdot \left[\frac{s_{i+1} - s_{i-1}}{2 \cdot \Delta x}\right] \cdot \left[\frac{c_{i+1} - c_{i-1}}{2 \cdot \Delta x}\right] = \\
= \left(\frac{D_c'}{D_c}\right) \cdot \frac{(s_{i+1} - s_{i-1})(c_{i+1} - c_{i-1})}{4\Delta x^2}$$

so that now c_{i+1} and c_{i-1} have the same coefficient. In fact, we can also define

$$\frac{1}{2}U(s_{i+1}, s_{i-1}) = \left(\frac{D'_c}{D_c}\right) \frac{s_{i+1} - s_{i-1}}{2}$$

Returning to the complete equation, we get therefore

$$c_{i+1} - 2c_i + c_{i-1} + \left(\frac{D'_c}{D_c}\right) \cdot \frac{(s_{i+1} - s_{i-1})(c_{i+1} - c_{i-1})}{4} = A(s_i)c_i - B(s_i)c_a + B(s_i)c_i$$

$$c_{i+1} - 2c_i + c_{i-1} + \frac{U(s_{i+1}, s_{i-1})}{2}c_{i+1} - \frac{U(s_{i+1}, s_{i-1})}{2}c_{i-1} = A(s_i)c_i - B(s_i)c_a + B(s_i)c_i$$

$$\left[1 + \frac{U(s_{i+1}, s_{i-1})}{2}\right]c_{i+1} - \left[2 + A(s_i) + B(s_i)\right]c_i + \left[1 - \frac{U(s_{i+1}, s_{i-1})}{2}\right]c_{i-1} = -B(s_i)c_a$$

We have $N_x - 2$ equations of this type, namely for $i = 1, 2, ..., N_x - 2$. In order to close the system, we need two other equations and these are given by the boundary conditions, which we already anticipate are the periodic ones. Indeed, periodic boundary conditions can be inserted by means of the following two conditions:

1.
$$c_0 = c_{N_x-1} \iff c_0 - c_{N_x-1} = 0$$

2.
$$\dot{c}_0 = -\dot{c}_{N_x-1} \iff c_0 - c_1 + c_{N_x-1} - c_{N_x-2} = 0$$

In fact, for Condition 2, we can proceed again by discretizing the derivatives in the following way

$$\dot{c}_0 = -\dot{c}_{N_x - 1} \iff \\
\iff \frac{c_0 - c_1}{\Delta x} = -\frac{c_{N_x - 1} - c_{N_x - 2}}{\Delta x} \iff \\
\iff c_0 - c_1 = -(c_{N_x - 1} - c_{N_x - 2}) \iff \\
\iff c_0 - c_1 - c_{N_x - 2} + c_{N_x - 1} = 0$$

After grouping, one more time, the coefficient of c_i and $c_{i\pm 1}$ by defining

$$E(s_i) = -[2 + A(s_i) + B(s_i)]$$
; $W^{\pm}(s_{i-1}, s_{i+1}) = [1 \pm U(s_{i-1}, s_{i+1})]$

our system of equations can eventually be written as:

$$\begin{cases} c_0 - c_{N_x - 1} = 0 \\ W^+(s_0, s_2) \cdot c_2 + E(s_1) \cdot c_1 + W^-(s_0, s_2) \cdot c_0 = -c_a B(s_1) \\ \dots \\ W^+(s_{i-1}, s_{i+1}) \cdot c_{i+1} + E(s_i) \cdot c_i + W^-(s_{i-1}, s_{i+1}) \cdot c_{i-1} = -c_a B(s_i) \\ \dots \\ W^+(s_{N_x - 3}, s_{N_x - 1}) c_{N_x - 1} + E(s_{N_x - 2}) c_{N_x - 2} + W^-(s_{N_x - 3}, s_{N_x - 1}) c_{N_x - 3} = -c_a B(s_{N_x - 2}) \\ c_0 - c_1 - c_{N_x - 2} + c_{N_x - 1} = 0 \end{cases}$$

The system just presented can be easily solved with linear algebra methods and the solution is the hydrogen concentration in soil in the quasi steady-state approximation, as

we want. Moreover, it is also quite simple to change the boundary conditions, one only needs to substitute the first and the last equations of the system with the ones describing the new set of boundary conditions. As an example, if Neumann BCs are preferred (with zero flux at the boundaries), it is only necessary to use the two following equalities

1.
$$\dot{c}_0 = 0 \iff c_0 - c_1 = 0$$

2.
$$\dot{c}_{N_x-1} = 0 \iff c_{N_x-1} - c_{N_x-2} = 0$$

instead of the ones for periodic BCs, while the rest of the system remains unchanged.

A.2 2D case

Now that we derived the 1D quasi-steady state approximation with the Finite Difference Method, we can quite easily extend it in 2D. In fact, the equation we need to solve is now:

$$\nabla^2 c + \frac{D_c'}{D_c} (\vec{\nabla} s) \cdot (\vec{\nabla} c) = -\frac{F(s, c) - Z_r \cdot BD(s, c)}{nZ_r (1 - s)D_c}$$
(A.3)

which is still a Poisson-like equation, similar to (A.1), but in more dimensions. The only change we have to take into account is that the discrete grid is now 2-dimensional and each position is identified by two indices, i and j along, respectively, the x and y direction. Hence, the finite difference approximation for the derivatives (that in 2D are a laplacian and a product of gradients) becomes

$$\begin{split} \nabla^2 c(x,y) &= \frac{\partial^2 c(x,y)}{\partial x^2} + \frac{\partial^2 c(x,y)}{\partial y^2} = \\ &= \frac{c(x+\Delta x,y) - 2c(x,y) + c(x-\Delta x,y)}{\Delta x^2} + \\ &+ \frac{c(x,y+\Delta y) - 2c(x,y) + c(x,y-\Delta y)}{\Delta y^2} \end{split}$$

and, already considering a symmetric form as in the 1D case,

$$\begin{split} (\vec{\nabla}s) \cdot (\vec{\nabla}c) &= \frac{\partial s(x,y)}{\partial x} \cdot \frac{\partial c(x,y)}{\partial x} + \frac{\partial s(x,y)}{\partial y} \cdot \frac{\partial c(x,y)}{\partial y} = \\ &= \frac{s(x + \Delta x, y) - s(x - \Delta x, y)}{2\Delta x} \cdot \frac{c(x + \Delta x, y) - c(x - \Delta x, y)}{2\Delta x} + \\ &+ \frac{s(x, y + \Delta y) - s(x, y - \Delta y)}{2\Delta y} \cdot \frac{c(x, y + \Delta y) - c(x, y - \Delta y)}{2\Delta y} \end{split}$$

Using the grid indices and considering for the sake of simplicity $\Delta x = \Delta y$, we can rewrite these derivatives as

$$\nabla^2 c(x,y) = \frac{c_{i+1,j} - 2c_{i,j} + c_{i-1,j}}{\Delta x^2} + \frac{c_{i,j+1} - 2c_{i,j} + c_{i,j-1}}{\Delta y^2} =$$

$$= \frac{c_{i+1,j} + c_{i,j+1} - 4c_{i,j} + c_{i-1,j} + c_{i,j-1}}{\Delta x^2}$$

and

$$(\vec{\nabla}s) \cdot (\vec{\nabla}c) = \frac{s_{i+1,j} - s_{i-1,j}}{2\Delta x} \cdot \frac{c_{i+1,j} - c_{i-1,j}}{2\Delta x} + \frac{s_{i,j+1} - s_{i,j-1}}{2\Delta y} \cdot \frac{c_{i,j+1} - c_{i,j-1}}{2\Delta y} =$$

$$= \frac{(s_{i+1,j} - s_{i-1,j}) \cdot (c_{i+1,j} - c_{i-1,j})}{4\Delta x^2} + \frac{(s_{i,j+1} - s_{i,j-1}) \cdot (c_{i,j+1} - c_{i,j-1})}{4\Delta x^2}$$

Substituting these quantities into Eq. (A.3) we get

$$\frac{c_{i+1,j} + c_{i,j+1} - 4c_{i,j} + c_{i-1,j} + c_{i,j-1}}{\Delta x^2} + \frac{D'_c(s_{i,j})}{D_c(s_{i,j})} \left[\frac{(s_{i+1,j} - s_{i-1,j}) \cdot (c_{i+1,j} - c_{i-1,j})}{4\Delta x^2} \right] + \frac{D'_c(s_{i,j})}{D_c(s_{i,j})} \left[\frac{(s_{i,j+1} - s_{i,j-1}) \cdot (c_{i,j+1} - c_{i,j-1})}{4\Delta x^2} \right] = -\frac{F(s_{i,j}, c_{i,j}) - Z_r \cdot BD(s_{i,j}, c_{i,j})}{nZ_r(1 - s_{i,j})D_c(s_{i,j})} \right]$$

To group the various coefficients in a better way, we define, similarly to the 1D case, the quantities:

$$U_x(s_{i+1,j}, s_{i-1,j}) = \frac{D'_c(s_{i,j})}{D_c(s_{i,j})} \left(\frac{s_{i+1,j} - s_{i-1,j}}{2}\right)$$

and

$$U_y(s_{i,j+1}, s_{i,j-1}) = \frac{D'_c(s_{i,j})}{D_c(s_{i,j})} \left(\frac{s_{i,j+1} - s_{i,j-1}}{2}\right)$$

while we can use the previously defined $A(s_{i,j})$ and $B(s_{i,j})$ since the right sides of equations (A.1) and (A.3) are the same, apart from the fact that in 2D s is labelled with two indices. Thus, we obtain:

$$\left(1 + \frac{U_x(s_{i+1,j}, s_{i-1,j})}{2}\right) c_{i+1,j} + \left(1 + \frac{U_y(s_{i,j+1}, s_{i,j-1})}{2}\right) c_{i,j+1} - \left[4 + A(s_{i,j}) + B(s_{i,j})\right] c_{i,j} + \left(1 - \frac{U_x(s_{i+1,j}, s_{i-1,j})}{2}\right) c_{i-1,j} + \left(1 - \frac{U_y(s_{i,j+1}, s_{i,j-1})}{2}\right) c_{i,j-1} = -B(s_{i,j}) c_a$$

Lastly, we can define

•
$$E(s_{i,j}) = -[4 + A(s_{i,j}) + B(s_{i,j})]$$

•
$$W_x^{\pm}(s_{i-1,j}, s_{i+1,j}) = [1 \pm U_x(s_{i-1,j}, s_{i+1,j})]$$

•
$$W_y^{\pm}(s_{i,j-1}, s_{i,j+1}) = [1 \pm U_y(s_{i,j-1}, s_{i,j+1})]$$

and eventually obtain

$$W_x^+(s_{i-1,j}, s_{i+1,j}) \cdot c_{i+1,j} + W_y^+(s_{i,j-1}, s_{i,j+1}) \cdot c_{i,j+1} - E(s_{i,j}) \cdot c_{i,j} +$$

$$+ W_x^-(s_{i-1,j}, s_{i+1,j}) \cdot c_{i-1,j} + W_y^-(s_{i,j-1}, s_{i,j+1}) \cdot c_{i,j-1} = -B(s_{i,j})c_a$$

We have $N_x \cdot N_y - 2(N_x + N_y) + 4$ equations of this type, one for each of the internal points of our discrete spatial grid, and $2(N_x + N_y) - 4$ boundary conditions for the points found on both the horizontal and vertical edges of the domain. Again, in this work, we choose periodic BCs so that the $2(N_x + N_y) - 4$ boundary conditions can be written as those previously discussed for the 1D case. Thus, we can build a system of $N_x \cdot N_y$ easily solvable with linear algebra methods and whose solution is the H_2 concentration in soil in the quasi-steady state approximation in 2 dimensions.

Acknowledgements

Rarely in this adventure, I took the time to thank in the proper way those who have helped me the most with their presence and love. Hence, this even more rare page of speech is for you. I know it is not barely sufficient, but any number of pages wouldn't be and, moreover, I studied physics, so, more than one page of me talking in full flow might be lethal.

In the beginning, I want to thank my family, my mum and dad, my brothers Francesco and Alice, and all my relatives, who, besides having given me the possibility to continue my studies, have always believed in me for real, supporting and tolerating with their love my frequent (and sometimes prolonged) period of silence and bad mood.

Another very important thanks goes to my kaleidoscopic group of friends: Aba, Serghio, Albi, Zordi, Capitano, Matte, Supremo, Teo, Eli, Sam, Pata, Fede, Manu, Dani, Chiara, Giada, Irene, Edo, Emma, Giulia, Tino, Zoe, Mela. Our countless adventures and moments together have amused, taught and helped me a lot in my life journey and will, I'm sure, in the future. Especially in these six years of university during which the afternoons in the library, the soccer and beach volley matches and, above all, the hangings at the Panke, in their simplicity and spontaneity, have made me feel part of something. Although, lately, each of us has started to walk his or her own path, as naturally happens, our friendship remains for me as solid as a covalent bond.

A special thanks to Politecnico of Turin and to my two supervisors, Professor Ridolfi and Professor Bertagni. Often, at the end of our emails, I wrote "thanks for your time and your advices" and it was not only a mere and formal way of conclusion: I really mean it and your kind guide has been precious.

A great thanks also to Andrea and Amedeo, my friends and colleagues during this long and winding journey among nice tricks, tight bindings and breakings of the symmetry. I must say, at the end of the day, the approximation has worked remarkably well.

Last but not least, a thanks to the young group of the up55, whose growing friendship is for me a source of hope (and risks!!).

Each adventure comes to an end and it is high time for this to be over. It has been a long journey, sprinkled with incredible memories, great satisfactions but also errors and stressful moments. Surely, the road has been full of non-linearities, turbulence and quantum traps. However, thanks to the vicinity of you all, I manage with these difficulties and come to a wonderful end. At least for now. Sooner, in fact, a new chapter will start and it is going to be closely linked to this one which is finishing. Thus, it is the perfect case to say:

To be continued...

Bibliography

- [1] M. B. Bertagni, F. Paulot, and A. Porporato. Moisture fluctuations modulate abiotic and biotic limitations of h2 soil uptake. *Global Biogeochemical Cycles*, 35(12):e2021GB006987, 2021.
- [2] R. Conrad and W. Seiler. Decomposition of atmospheric hydrogen by soil microorganisms and soil enzymes. *Soil Biology and Biochemistry*, 13(1):43–49, 1981.
- [3] S. Lawrence Dingman. *Physical hydrology*. Waveland press, 2015.
- [4] D. H. Ehhalt and F. Rohrer. The dependence of soil h2 uptake on temperature and moisture: a reanalysis of laboratory data. *Tellus B: Chemical and Physical Meteorology*, 63(5):1040–1051, 2011.
- [5] F. Laio, A. Porporato, L. Ridolfi, and I. Rodriguez-Iturbe. Plants in water-controlled ecosystems: active role in hydrologic processes and response to water stress: Ii. probabilistic soil moisture dynamics. Advances in water resources, 24(7):707–723, 2001.
- [6] P. Moldrup, T. K. K. Chamindu Deepagoda, S. Hamamoto, T. Komatsu, K. Kawamoto, D. E. Rolston, and L. W. de Jonge. Structure-dependent water-induced linear reduction model for predicting gas diffusivity and tortuosity in repacked and intact soil. *Vadose Zone Journal*, 12(3):vzj2013-01, 2013.
- [7] P. Moldrup, T. Olesen, T. Yamaguchi, P. Schjønning, and D. E. Rolston. Modeling diffusion and reaction in soils: Ix. the buckingham-burdine-campbell equation for gas diffusivity in undisturbed soil. *Soil Science*, 164(8):542–551, 1999.
- [8] J. R. Nagel. Numerical solutions to poisson equations using the finite-difference method [education column]. *IEEE Antennas and Propagation Magazine*, 56(4):209–224, 2014.
- [9] L. A. Segel. Jd murray: Mathematical biology, volume i (an introduction) and volume ii (spatial models and biomedical applications). *Mathematical Medicine and Biology: A Journal of the IMA*, 20(4):377–378, 2003.
- [10] N. V. Smith-Downey, J. T. Randerson, and J. M. Eiler. Temperature and moisture dependence of soil h2 uptake measured in the laboratory. *Geophysical Research Letters*, 33(14), 2006.
- [11] S. Yonemura, M. Yokozawa, S. Kawashima, and H. Tsuruta. Model analysis of the influence of gas diffusivity in soil on co and h2 uptake. *Tellus B: Chemical and Physical Meteorology*, 52(3):919–933, 2000.